ABSTRACT

Title of Thesis: SCALES OF BANK ROUGHNESS AND THEIR RELATIONSHIP TO BANK EROSION PROCESSES

Erik Ravnholt Hankin, Master of Science, 2009

Thesis directed by: Dr. Karen L. Prestegaard
Department of Geology

Stream bank erosion rates and the stabilization of channel width are poorly understood processes. There have been two distinct approaches to the study and prediction of bank erosion rates in natural streams. In order to predict bank shear stresses, scientists either define a reach as being meandering or straight, even though most river channels are neither meandering nor straight but a combination of the two. This thesis aims to determine if river segments can be divided into straight reaches and curved reaches with different bank erosion prediction approaches applied to each as well as investigating the role of bank roughness element size and spacing in bank erosion. The results show that straight reaches are affected by upstream curvature and that large isolated bank protrusions that are widely spaced generate erosion-causing, stable, macroturbulent eddies. The thesis has implications for stream restoration practices regarding bank stability and erosion.

SCALES OF BANK ROUGHNESS AND THEIR RELATIONSHIP TO BANK EROSION PROCESSES

by

Erik Ravnholt Hankin

Thesis submitted to the Faculty of the Graduate School of the
University of Maryland at College Park in partial fulfillment
of the requirements for the degree of
Master of Science
2009

Advisory Committee:

Dr. Karen L. Prestegaard, Chair
Dr. Philip M. Piccoli
Dr. Andrew H. Baldwin

Table of Contents

List of Tables

List of Figures

Introduction

Stream bank erosion is a natural geomorphic process that occurs during high discharges due to fluvial erosion, or during the recession limb of hydrographs due to high pore water pressure and bank failures. Bank erosion is difficult to predict due to the numerous bank properties that affect erodibility including: bank material weight and texture, shear and tensile strengths, groundwater level (pore water pressure), permeability, stratigraphy, geometry, and roughness (Abernethy and Rutherford, 1998). With such a wide range of factors contributing to bank erosion, it is useful to consider bank erosion in terms of broad process categories. Julian and Torres (2005) identify three bank erosion process domains: subaerial preparation; fluvial entrainment of bank sediment; and mass failure mechanisms. Depending upon the channel characteristics, different erosion process domains will dominate. Subaerial preparation is the primary cause of bank erosion in first order streams and the furthest upstream reaches, while fluvial entrainment and mass failure dominate in mid-basin areas (Lawler, 1995). This is because streams in upper reaches, while flowing down steep slopes, have low discharges and depths. The higher discharges of lower reaches are often offset by low gradients and shear stresses. As a result, depth and slope combine to produce peak levels of hydraulic erosivity in the mid-reaches of watersheds. Thus, the stability of banks in middle reaches is thought to be largely determined by shear forces acting on surficial grains. This shear stress acting upon the banks is resisted by the strength of the material on the bank (which is affected by grain size, cohesiveness, and pore water pressure) and bank roughness, which is often influenced by vegetation.

Although it is generally viewed and treated as a river management problem, bank erosion is a natural process that provides necessary geomorphic and ecological functions by providing a sediment source that creates riparian habitat; maintaining diverse natural structure and habitat function; acting as a mechanism for the input of large woody debris; and modulating changes in channel morphology and pattern (Florsheim et al., 2008). In many urban watersheds, however, an increase in high flows has accelerated rates of bank erosion causing channel enlargement (Hammer, 1972). Bank erosion is one of the major sources of sediment and nutrients in the Chesapeake Bay Watershed, which has caused numerous dead zones throughout the Bay and its larger tributaries. Stream bank erosion processes, rates, and the stabilization of channel width are poorly understood. Active bank erosion processes in the Chesapeake watershed provide a natural laboratory in which to examine bank erosion.

Traditionally, there have been two distinct approaches to the study and prediction of bank erosion rates for natural systems. Scientists and engineers either classify a channel as being curved or straight. For curved channels, bank erosion is often predicted as a function of the radius of curvature and channel width (Nanson and Hickin, 1986). In straight reaches, the shear stress is partitioned into bed and bank components using procedures derived from flume channels (e.g. Flintham and Carling, 1988). The problem with these approaches is that few rivers can be defined as one of the two end members and the extent of applicability of the approaches has not been defined.

In addition to channel morphology, bank roughness, generated by vegetation or large particles, plays a major role in the prediction of bank shear stresses and erosion. It has been well documented that riparian vegetation can stabilize stream banks, largely by

adding “root cohesion” to the soil cohesion. Trees and herbaceous vegetation can also potentially destabilize channel banks due to wind throw or hydraulically by generating eddies. It is important to understand the effect of the presence of riparian vegetation on each of the three erosion process domains (subaerial, hydraulic, mass failure) that occur from upstream to downstream within watersheds.

Vegetation can both cause and prevent subaerial erosion. In the case of windthrown trees, riparian vegetation is actually causing subaerial erosion. However, this is dependent on the rooting depth of trees, and its presence decreases downstream. Vegetation is much more likely to prevent subaerial preparation. Freeze/thaw cycles can cause subaerial erosion. However, vegetation is able to prevent or reduce this type of erosion because it limits fluctuations in soil temperature by lowering the surface and velocity and the turbulent exchange of heat between the soil surface and the atmosphere (Bohn, 1989). Bohn discovered that even sparse grass cover in upland environments protects river banks from freeze/thaw cycles. Because the development of needle ice is highly increased with an increase in the number of freeze/thaw cycles and causes erosion, riparian vegetation is highly effective at mitigating almost all of the effects of desiccation. Roots bind bank material together and resist cracking, and grass and leaf littler reduce drying (Abernethy & Rutherford, 1998). Thus, vegetation can reduce the amount of subaerial erosion on the banks of upper reaches of streams.

The hydraulic effects of vegetation in the flow are extremely complex, and, therefore, it is difficult to predict the degree to which vegetation will affect erosion on the stream bank. However, it can still be noted that vegetation increases the roughness of the bank, thereby decreasing the velocity along the bank. This, in turn, decreases the shear

velocity and shear stress along the stream bank, decreasing the erosion along the bank (Ritter *et al*., 2002). Yet the effect is local and scale dependent. As the size of the channel increases relative to the size of bank vegetation, the hydraulic effects of bank vegetation may be diminished. Abernethy and Rutherford (1998) found that revegetating a bare channel and reintroducing a pre-disturbance load of large woody debris to the flow will have the greatest effect on the reducing fluvial entrainment of sediment along the bank in upper reaches of river systems.

Like subaerial preparation, vegetation can have a positive or a negative correlation with mass failure. The weight of a tree can increase the risk of the bank slumping into the stream. However, this is entirely dependent on the species of tree and the size of its roots and rootballs (Abernethy & Rutherford, 1998). As previously mentioned, drier banks are more stable than banks with high water tables and therefore, high pore water pressures. . Consequently, the effects of evapotranspiration and improved bank drainage due to the presence of riparian vegetation on the bank are likely to maintain drier conditions. Trees on the bank can affect antecedent moisture conditions in the bank, which may reduce the risk of mass failure (Thorne, 1991). However, the roots of trees provide the greatest effect on the mass stability of stream banks and subsequent prevention of mass failure.

Bank protrusions, which includes tree trunks, rootwads, and rip-rap, may contribute to bank roughness, but they can also generate macroturbulent eddies (Raupach, 1992). These eddies bring high velocities near the bank, thus creating non- logarithmic velocities profiles out from the bank that do not follow the von Karman's Law of the

Wall. The new velocity profile can result in high near-bank velocities and shear stresses, resulting in bank erosion.

Many studies simplify bank roughness when predicting bank erosion by using a Manning's roughness coefficient or an average bank roughness size. The problem with this is that roughness varies along a stream bank. Smaller roughness elements may stabilize the bank, while the largest may cause erosion by generating stable, macroturbulent eddies. In addition to size, spacing of the roughness elements also determines how bank roughness affects the flow. Isolated roughness elements may also generate macroturbulent eddies. Therefore, it is necessary that one make a detailed investigation of the bank roughness elements size and spacing when predicting bank shear stresses.

The objectives of this research are as follows:

1. To determine if river segments can be divided into straight reaches and curved reaches and if different bank erosion prediction approaches may be applied to each.
2. To create a method for physically measuring bank roughness that can be used in place of roughness estimates, such as Manning's *n* or the average bank roughness.
3. To determine conditions under which stream bank roughness, specifically the size and spacing of bank protrusions, generate stable, macro-turbulent eddies that affect near bank velocities, shear stress, and bank erosion.

In order to help determine if sections of rivers can truly be classified as either straight reaches or curved reaches, a study was conducted on the East Fork River, Wyoming. The

study used data from Prestegaard (1982) to calculate bank shear stress values using two separate methods: the Einstein method (Einstein and Barbarossa, 1951), which uses measurements of the velocity field to partition the shear velocity into bank and bed components, and the Carling method (Flintham and Carling, 1988), which uses the channel dimensions to partition the shear stress into bank and bed components. The Einstein method requires more data, but is not limited to a given channel shape, while the Carling method is designed for straight, trapezoidal channels. The 100-meter study reach is straight, but is located approximately 20 meters downstream of a meander bend. The main goal of the study is to determine if upstream meanders affect the downstream straight reaches, thereby testing whether sections of rivers can be classified as either being straight or meandering for erosion prediction purposes.

Another study was conducted to investigate the role of bank roughness in the creation of macroturbulent eddies. In order to conduct the study, a method for physically measuring bank roughness, as opposed to using a Manning's roughness coefficient or the average bank roughness, was developed. The study sites included natural and stabilized sections of the Anacostia River, a region where urbanization has exerted significant stresses on the channel, resulting in high rates of bank erosion (Behrns, 2007). The purpose of this part of the study is to determine roughness height distributions and the size and spacing of roughness heights that generate macroturbulent eddies. During high flows, macroturbulent eddies formed at isolated roughness elements. These eddy lengths were measured and compared with the physical roughness size at the gauge height at the time of the eddy generation. These eddy lengths were then compared with eddy lengths predicted from Raupach's (1992) study of drag partition on rough surfaces. The

predicted eddy lengths were compared with the measured eddy lengths and analyzed alongside the hydrologic data to evaluate conditions under which macroturbulent eddies occur.

These two studies, taken together, can provide important information on the influence of roughness heights and spacing on bank stability and can provide constraints on how to use shear stress partitioning procedures for natural channels. This information is needed because there is significant interest in stabilizing stream reaches with trees and other bank vegetation or rootwads, both of which can generate macroturbulent eddies if not carefully emplaced.

Prediction of Bank Shear Stress

Introduction

Bank erosion is a complex phenomenon in which numerous factors play a role. In general, stream hydraulics, sediment transport mechanisms, bank properties, and vegetation determine both styles and rates of bank retreat (Nanson and Hickin, 1986). The numerous bank properties that affect erodibility include bank material weight and texture, shear and tensile strengths, groundwater level (pore water pressure), permeability, stratigraphy, geometry, and roughness characteristics (Abernethy and Rutherford, 1998). With such a wide range of factors contributing to bank erosion, it is useful to consider bank erosion in terms of broad process categories. Three bank erosion process domains can be identified: subaerial preparation; fluvial entrainment of bank sediment; and mass failure mechanisms (ASCE, 1998; Julian and Torres, 2005).

There have been two distinct approaches to the study and prediction of bank erosion rates in natural streams. Scientists and engineers have long noticed that the highest bank erosion rates are located on the outside of meander bends, due to the location of the maximum flow velocities (Leighly, 1936). Thus, one major approach to predicting bank erosion is to create relationships between bank curvature and bank erosion (e.g. Jang and Shimizu, 2005; Nanson and Hickin, 1983, 1986; Hudson and Kesel, 2000). Many streams, however, are not meandering, and bank erosion rates are predicted by assuming that the river is straight and partitioning shear stress into bed and bank components (e.g. Knight et al., 1984; Flintham and Carling, 1988). Most of these methods of shear stress partitioning have come from flume studies and do not incorporate

either macroturbulent eddies or significant bank roughness that results from bank vegetation. These two distinct approaches for the prediction of bank erosion are for the two end-member cases: meandering reaches and straight reaches, even though most river channels are neither truly meandering nor straight. What is needed, therefore, is an evaluation of the applicability of these methods for stream channels that are not one end-member or another.

The purpose of this section is to investigate the methods for predicting shear stress along the banks of relatively straight reaches with little vegetative bank roughness. The hypothesis to be tested is that river segments can be divided into straight reaches and curved reaches and that shear stress partitioning methods can be applied to the straight reaches to predict bank erosion, with meander migration techniques being applied to the curved reaches. The null hypothesis is that curved river segments affect the shear stress distribution of nearby, straight reaches.

Previous Research

Bank Erosion Processes in Curved Reaches of River

Research on bank erosion is complicated by the relationships between bank erosion and channel morphology. In meandering reaches, bank erosion rates are often related to channel curvature, using indices such as the radius of curvature to width ratio: (Rc/w). Leopold and Wolman (1957) compiled a database from highly meandering rivers and developed equations for both the Rc and w using the meander wavelength, λ:

$\lambda=10.9w^{1.01}$

$\lambda=4.7Rc^{0.98}$

Figure 1 provides a schematic diagram of the geometric parameters of a meander. The meander wavelength is scaled primarily by two parameters; the channel width, *w*, and the radius of curvature, *Rc*. The channel width reflects the size of the river (a function of basin area and bankfull discharge). The radius of curvature also affects the wavelength; tightly curved meander bends will have shorter wavelengths than open meander bends. The meander wavelength equations from Leopold and Wolman (1957) can be considered to be linear (exponents ~1). Therefore, the following relationships can be developed:

$Rc/w=(\lambda/4.7)/(\lambda/10.9)=10.9/4.7=2.3$

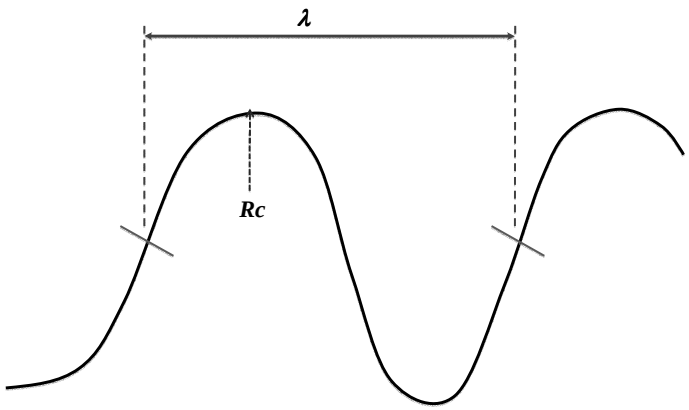

Figure 1: Geometric parameters of a meandering stream: λ is the wavelength and *Rc* is the radius of curvature.

Leopold and Wolman (1960) found that for highly meandering rivers, the average *Rc/w* ratio is between 2 and 3. This suggests that the relationship probably is a function of channel curvature exerting an influence on flow.

Bagnold (1960) showed that as the radius of curvature decreases, the flow tends to shift towards the outer bank, causing a decrease in resistance on the inside of the bend. Greater curvature will continue to lessen inner bank resistance until a critical *Rc/w* is attained, when flow along the inner bend becomes unstable and breaks away from the boundary. These conditions create eddy currents along the inside boundary, increasing the energy dissipation and, as a result, establishing low velocities and sediment deposition on the inside of channel bends. Several studies have related the *Rc/w* ratio to bank erosion rates through flume studies (Odgaard, 1989) or empirical studies that relate measured bank erosion rates to bend characteristics (Nanson and Hickin 1983; 1986). From their measurements, Nanson and Hickin generated two empirical equations to

predict erosion rates (m/yr) for tightly meandering rivers (*Rc/w* ~2.9). This is shown in Figure 2. Note that there are only two variables in this equation: *Rc/w* and scroll-bar spacing (*sp*), which is an empirical measure of sediment deposition rate (and thus sediment supply or transport rate). The channel width is part of a dimensionless number (*Rc/w*) so the actual size of the channel is not a parameter in this approach.

$$M\ (m/yr) = 0.05\ (Rc/w)^{2.05} + 0.00035\ sp^{2.63}$$ (for *Rc/w* ratios between 1.3 and 2.9)

$$M\ (m/yr) = 2.75/\ (Rc/w)^{1.73} + 0.00035\ sp^{2.63}$$ (for *Rc/w* ratios between 2.9 and 7)

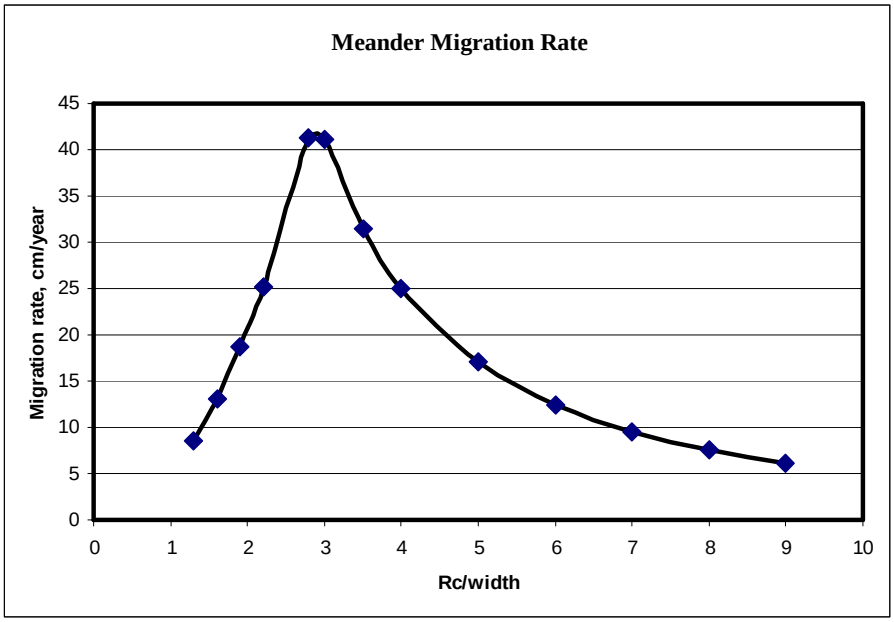

Figure 2: The relation of migration rate (cm/yr) to bend curvature ratio (*Rc/w*) (adapted from Nanson and Hickin 1983).

Hudson and Nessel (2000) also investigated the role of *Rc/w* with migration rates along the lower Mississippi River. They found that, unlike Nanson and Hickin, the highest rates of migration occurred with meander bends having a curvature between 1.0 and 2.0, which is a departure from the previous models. The complex flood-plain deposits in the lower Mississippi show relationships that deviate from the models derived in homogeneous flood-plain deposits. Hudson and Nessel, however, did not investigate or account for the role of sediment supply from upstream sources or the type of transport (bedload or suspended) in their discussion.

Bank erosion processes in straight reaches of river

For non-meandering streams, channel size and position in the watershed seem to affect bank erosion processes. The size of stream channels changes within a watershed. In most river basins, channel width increases more rapidly than channel depth (Leopold and Maddock, 1953). This means that most headwater streams are shallow, which leads to low channel shear stress and the stability of small, vertical stream banks (Lawler, 1995). Moving downstream from the drainage divide, the extent to which each process domain influences the bank erosion process changes. This is largely due to downstream changes in channel dimensions. Lawler (1995) suggests that subaerial mechanisms dominate the erosion process in small catchments. Hooke (1980) correlates bank erosion rates with river width, thus bank erosion rates are proportional to the size of the channel, or watershed area in the systems that she evaluated. In middle-order basins, fluvial entrainment processes generally dominate, and banks in larger catchments usually undergo retreat due to mass failure mechanisms.

Lawler (1995) stated that the prevailing mechanism of erosion along banks of mid-basin areas in many catchments is fluvial entrainment of bank sediments. This is because streams in upper reaches, while flowing down steep slopes, have low discharges and depths, but the higher discharges of lower reaches are more than offset by low bed-slopes. As a result, discharge and slope combine in middle reaches to produce peak levels of hydraulic erosivity. Thus, the stability of banks in middle reaches is thought to be largely determined by the balance of forces acting on surficial grains. This balance of forces is the shear stress acting upon the banks that is resisted by the strength of the material on the bank (which is affected by grain size, cohesiveness, and pore water pressure).

The shear stress acting on the bank can be directly measured by measuring velocity profiles out from the channel banks as long as the velocity distributions follow the logarithmic von Karman Law of the Wall:

$$U/U^* = 1/k \; x \; ln(z/z_o)$$

$$U = 2.5U^* ln(30z/K_s)$$

where U is the velocity, U^* is the shear velocity, k is the von Karman constant, z is distance from the bank or bed, z_o is $1/30^{th}$ of the roughness height, K_s. U^* is equal to the slope of the logarithmic relationship between U and z (Figure 3). The Law of the Wall states that the velocity changes logarithmically with distance from the bank or bed. An example of a logarithmic velocity profile measured near the surface as a function of

distance from the bank is shown in Figure 4. These data were collected at a low flow in Paint Branch Creek, Maryland.

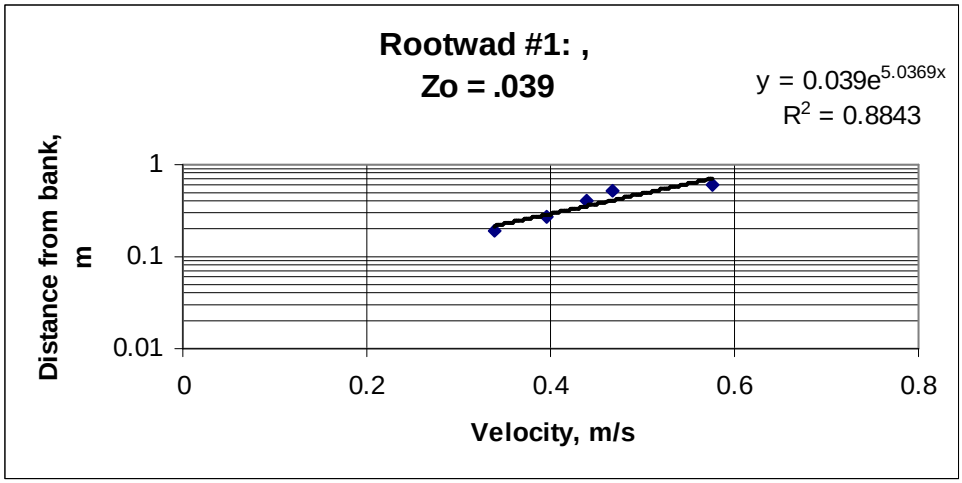

Figure 3: Law of the Wall. The velocity changes with the log of distance from the bank or bed. Bank roughness and bank shear stress can both be obtained from these measurements. The y intercept, or z_o, is related to the roughness height. The slope of the relationship is equal to $5.75U^*$ and is proportional to the shear stress on the bank; $\tau_{bank} = \rho(U^*_{bank})^2$, where ρ is the density of the fluid.

The direct measurement of velocity profiles near the bank is complicated by the formation of macroturbulent eddies near the wall, or internal distortion of the flow generated by channel bends. Macroturbulent eddies can generate flow structures in which the velocity does not increase with logarithmic distance away from the bank. This limits the accuracy of the measurements of shear stress near the bank. This problem is dealt with in flume studies by directly measuring shear stress along the banks by use of

pressure plates (e.g. Knight et al., 1984). Another approach to partitioning shear stress into bed and bank influenced areas is the Einstein and Barbarossa (1951) method, in which the entire cross section velocity structure is used to obtain U^* along the banks and bed. The partitioned shear velocity along the bank can then be used to calculate the shear stress along the bank.

For straight reaches, Flintham and Carling (1988) following Knight et al., (1984) designed a method to partition total boundary shear stress into bed and bank components by using the proportion of the boundary incorporated into the bank and bed. The total boundary shear stress for a uniform channel can be determined by:

$$\tau_o = \rho g R S$$

where τ_o is total boundary shear stress (N/m^2), R is hydraulic radius (area/perimeter), g is gravitational acceleration, and S is energy slope. These parameters are determined in the field by measurement of channel gradient and channel cross section.

Using Knight et al.'s (1984) model for predicting boundary shear stress in smooth, rectangular channels, Flintham and Carling (1988) developed equations to provide a simple method of determining the mean bed and bank shear stress in straight, symmetrical, and either trapezoidal or rectangular channels with varying degrees of bed and bank roughness. The equations were derived using a tilting flume with a bed consisting of well-sorted gravels. Local boundary shear stresses were measured using the Law of the Wall. For trapezoidal channels these equations are:

$$SF_{bank} = 1.77\{(P_{bed}/P_{bank}) + 1.5\}^{-1.4}$$

$$\tau_{bank} = \tau_o * SF_{bank}\,(B+P_{bed})/(2*P_{bank})$$

where SF_{bank} is the shear force on the bank, P denotes perimeter, and B is the surface width.

In terms of model application, Flintham and Carling state that the model should be applied to large-scale channels with caution due to Reynold's numbers likely exceeding the upper limit of the experimental range. The model is suitable for straight channels with bank slopes between 45^o and 90^o with minimal effects from skew-induced secondary currents. Canalized waterways and riffle-sections in straight gravel-bed rivers are examples of appropriate field channels.

This approach for shear stress partitioning has been widely used in the prediction of bank erosion and the development of morphology in rivers. As flow depth and velocity increases, shear stresses that are exerted on the bank can entrain particles. Particle entrainment, or basal erosion due to fluvial hydraulic force, thus depends upon the ratio of the shear stress to the resisting forces of the bank. For banks with homogeneous sediment, this can be expressed as a critical entrainment Shields' parameter for the bank sediments (Duan, 2005):

$$\tau^*_{crit} = 4/3C'_L\,(cosB + ((\rho_s/(\rho_s-\rho)g)fc$$

where C'_L is the coefficient of the lift force: $C'_L = C_L \, ln2(0.35dK_s/k^2$

K_s = roughness height, k = von Karman's constant, d= depth, B is bank slope, and fc is cohesion of the bank material.

Study Site and Methods

This study used data obtained from Prestegaard's (1982) research on the East Fork River, Wyoming. The river consists of tight meander bends and long, straight reaches (Figure 4). The wavelength of the meander bends is 18-22 channel widths, significantly higher than the 11 channel widths identified by Leopold and Wolman (1960) for classical meandering reaches. The banks consist primarily of sand-sized particles and have very low bank roughness. Velocity profiles across the channel were measured at 3 cross section locations, labeled 1610, 1573, and 1533, in a straight reach downstream of a bend (Figure 5). The *Rc/w* of the bend is 1.3. The 1533 transect is over 100 meters downstream of this bend. The measurements were primarily made during the falling limb of the snowmelt hydrograph in June and July 1980 (Figure 6). Background information about this river can be found in Prestegaard (1982) and Leopold and Emmett (1997).

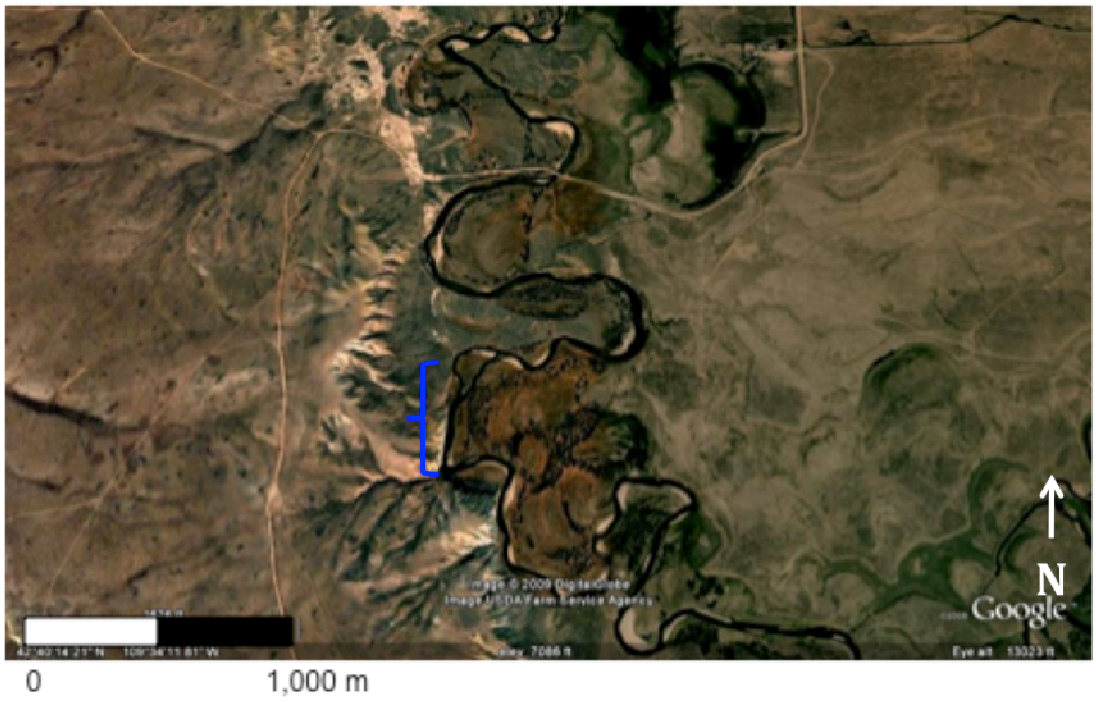

Figure 4: Aerial photograph of the East Fork River, Wyoming data provided by Google Earth from USDA. A scale bar is provided in the lower left hand portion of the figure. The river shifts between tight meanders bends connected by straight reaches. The study reach is highlighted in blue. A north arrow is provided in the lower right-hand portion of the figure.

Water surface elevation data were obtained from water surface gauges that were monitored during the time period that the velocity profiles were obtained. These gauges were surveyed to a common datum. Figure 6 shows the water surface elevation data for these 3 gauges.

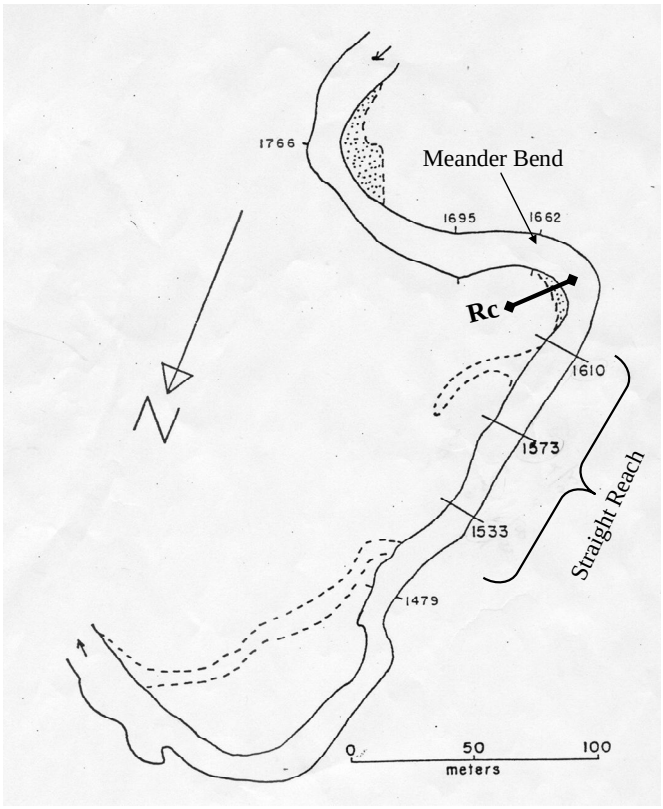

Figure 5: Map of Prestegaard (1982) study site that shows the cross section locations, 1610, 1573, and 1533 (used by permission).

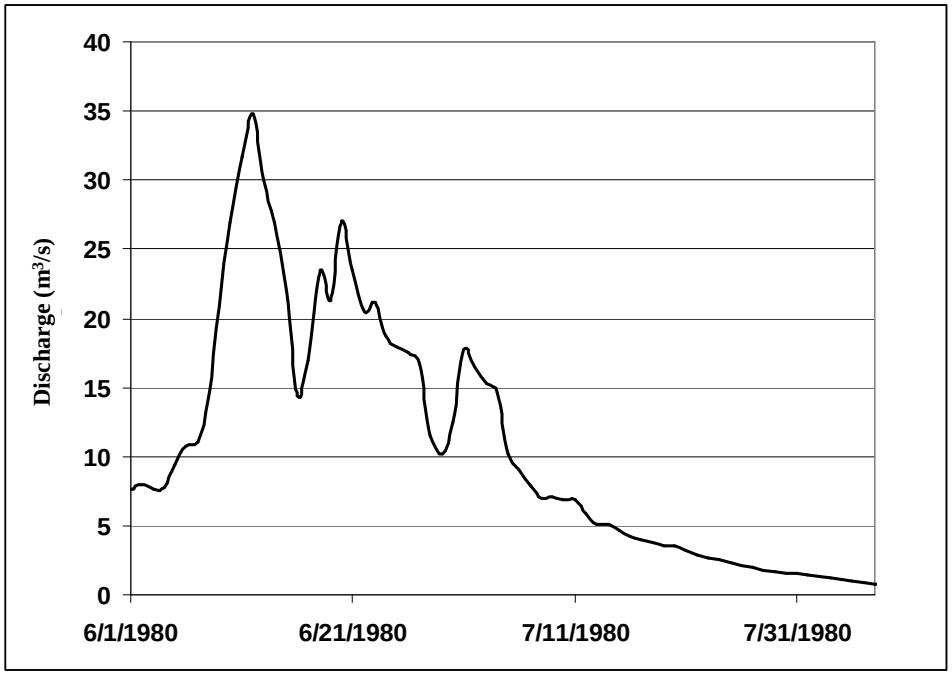

Figure 6: Snowmelt hydrograph for the East Fork River, 1980. USGS gauge 09203000. Prestegaard (1982) measurements were made between 6/17/1980 and 7/7/1980.

(A)

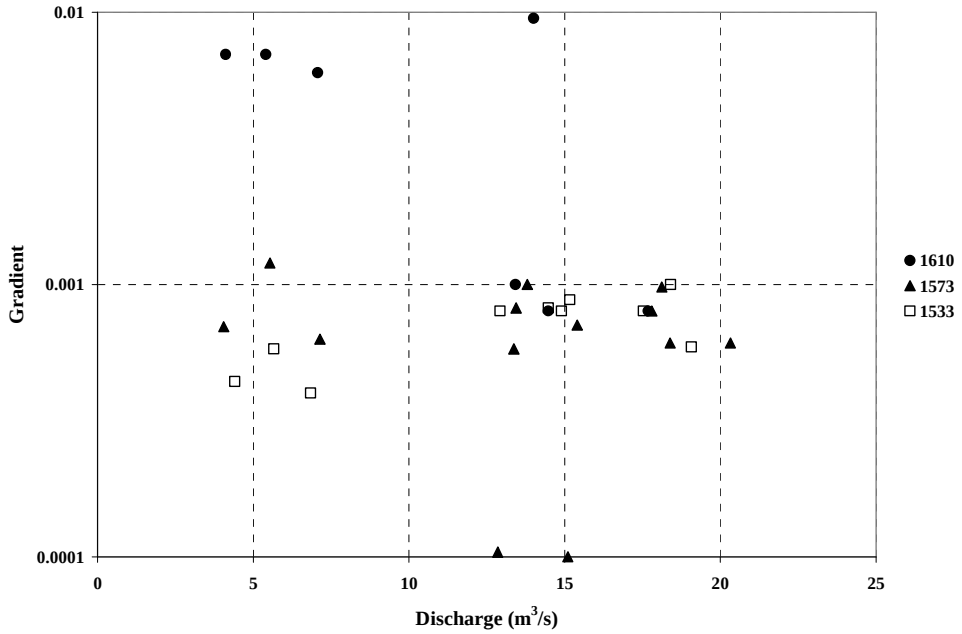

(B)

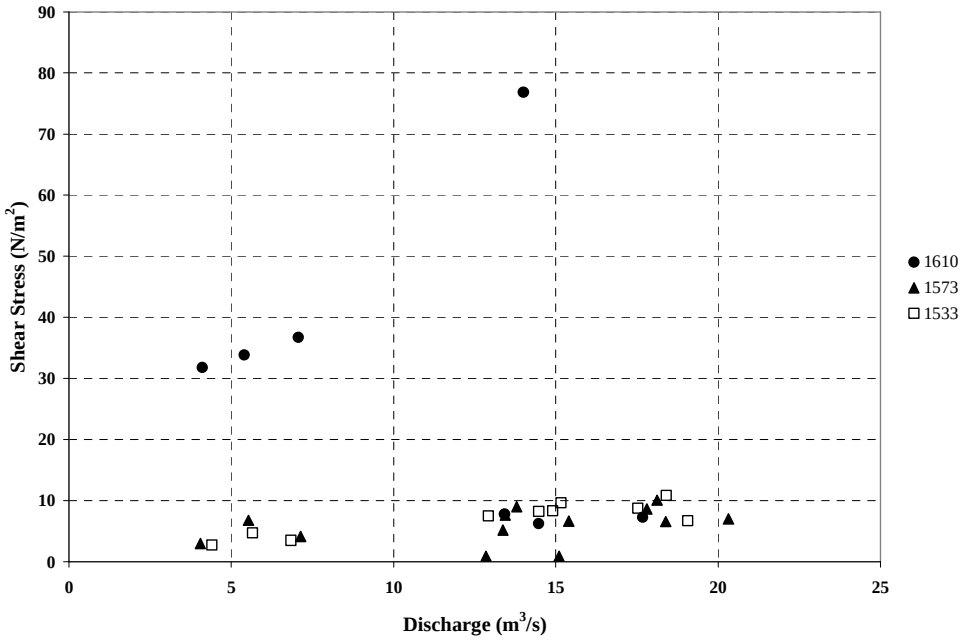

Figure 7: Water surface elevation data and total boundary shear stress for the three gauges. 1610 is the site closest to the meander bend with sites 1573 and 1533 further

downstream, respectively. Gradient (A) and average boundary shear stress (B) versus discharge.

Because there were macroturbulent eddies along the bank downstream of the bend, the Law of the Wall could not be used to calculate the bank shear stress. Instead, isovels were measured and the Einstein method was used to partition the shear velocity into bed and banks components. The shear velocities along the bank were then used to caluculate the bank shear stresses $\tau_{bank} = \rho(U^*_{bank})^2$ (Figure 8). Using the perimeter, hydraulic radius, and gradient data from Prestegaard (1982), the Flintham and Carling approach (see above) was also used to predict the bank shear stresses at the three transects.

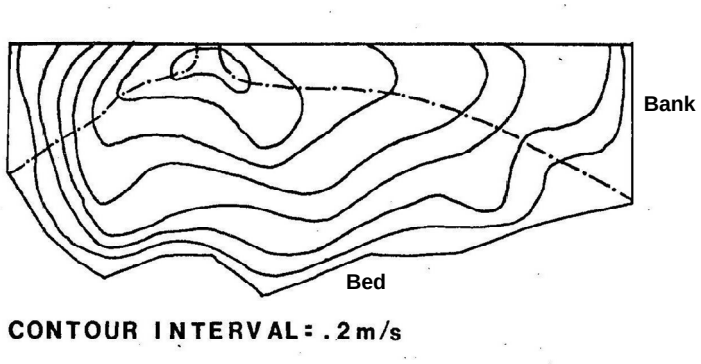

Figure 8: Example of the use of the velocity flow field, illustrated by isovels that were used by Prestegaard (1982) to partition U^* into bed and bank components using the Einstein-Barbarossa method of shear stress calculation (used by permission).

Results

Shear Stress Prediction

Using the velocity data from Prestegaard (1982), bank shear stress values for the three transects were calculated. Table 1 shows the range of left and right bank shear stress values over the study period for the upstream transect, which was at the channel bend.

Table1. Range of shear stress values along the left (τ_{lb}) and right (τ_{rb}) banks of the 1610 transect on the East Fork River. The 1610 site is the furthest upstream and closest to the upstream meander bend.

Discharge (m^3/s)	**τ_{lb} (N/m^2)**	**τ_{rb} (N/m^2)**
473.9	9.03	51.5
624.4	15.6	81.8
511.1	15.4	41.2
190.7	8.3	12.3
494.5	13.0	22.0
249.7	10.2	15.1
145.2	10.2	9.8

The perimeter, hydraulic radii, and gradient data from Prestegaard (1982) were then used to predict the bank shear stresses for the same flows using the Flintham and Carling approach (Table 2). After calculating both the Einstein and Carling shear stresses, the results could be compared in order to see if the Carling method was a fair predictor of shear stress along the banks.

Table 2. Range of predicted bank shear stress values for the 1610 transect on the East Fork River calculated using the Flintham and Carling approach.

Discharge (m^3/s)	Carling τ_{lb} (N/m^2)	Carling τ_{rb} (N/m^2)
473.9	4.90	10.9
624.4	4.66	8.43
511.1	3.86	8.78
190.7	23.4	40.7
494.5	52.1	36.8
249.7	22.1	20.7
145.2	18.2	22.0

Shear Stress Comparison

The shear stress values calculated by the two methods for each of the two banks at the three cross sections were compared. The reach is characterized by a bend, followed by a straight reach, therefore we expect to see deviations between the Flintham-Carling and Einstein-Barbarossa approaches at the bend, but similar values for the reach downstream of the bend. A one to one ratio would signify that the Flintham and Carling approach was a good predictor of bank shear stress obtained from velocity data. Figure 9 shows the two sets of calculated shear stresses for all three sites for the left bank (A) and right bank (B).

(A)

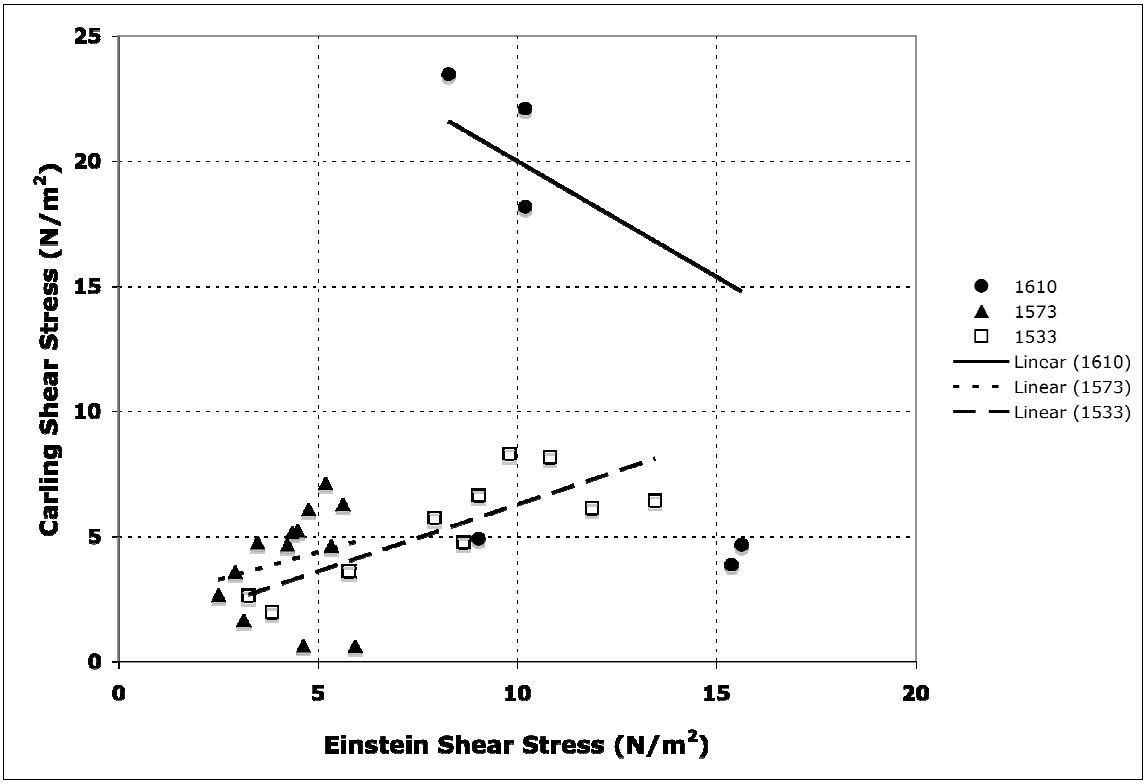
Carling Shear Stress (N/m2)
Einstein Shear Stress (N/m2)
0
5
10
15
20
25
1610
1573
1533
Lincar (1610)
Linear (1573)
Linear (1533)

(B)

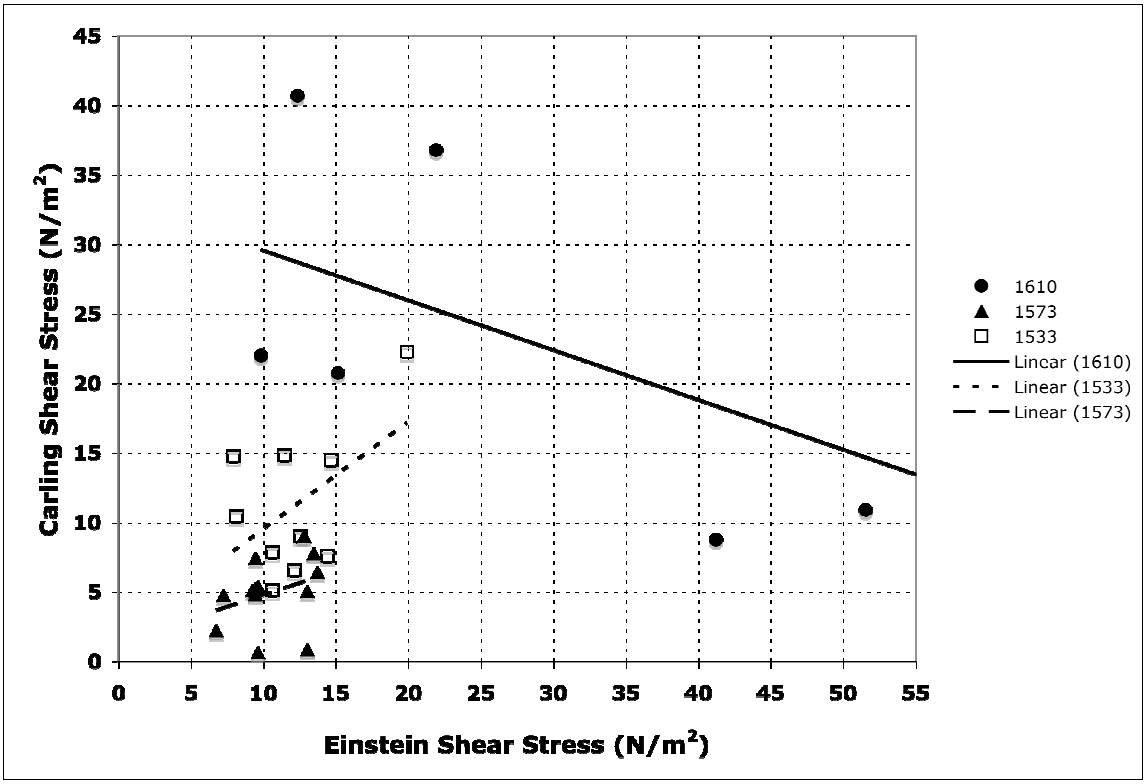

Figure 9: Comparison of Flintham and Carling shear stresses with Einstein shear stresses on the left (A) and right (B) banks. 1610 is the site closest to the meander bend with sites 1573 and 1533 further downstream, respectively. The trendline equations and R^2 values for the sites can be found in Table 3.

Table 3. Equations and R^2 values for the trendlines in Figure 9, where Flintham and Carling shear stresses were compared with Einstein shear stress on both banks.

Site	**1610** (upstream)	**1573** (middle)	**1533** (downstream)
Left Bank Equation	y = -0.93x + 29.3	y = 0.44x + 2.18	y = 0.53x + 0.95
Left Bank R^2	0.026	0.050	0.676
Right Bank Equation	y = -0.36x + 33.1	y = 0.34x + 1.38	y = 0.77x + 1.90
Right Bank R^2	0.514	0.106	0.265

The data suggest a best-fit line with a slope of one would indicate that the Flintham and Carling approach was an equal predictor of bank shear stress as the Einstein method. None of the trendlines for either bank at any of the three sites had a slope of one. Going downstream, the slopes go from negative values to a high of 0.76. The highest slope is found on the right bank, the bank inside the upstream meander bend, at 1533, the site furthest downstream from the bend.

Ratios of the shear stress values calculated for each individual flow at each site using both methods were then determined in order to see if the Carling approach generally over or underpredicted the shear stress on the banks. This data is present in Table 4.

Table 4. Ratios of Einstein shear stresses to Flintham and Carling shear stresses for a range of flows at all three sites.

Site	Discharge (m^3/s)	τ_{lb} Ratio	τ_{rb} Ratio
1610 (upstream)	13.4	1.8	4.7
	17.7	3.3	9.7
	14.5	4.0	4.7
	5.4	0.4	0.3
	14.0	0.2	0.6
	7.1	0.5	0.7
	4.1	0.6	0.4
1573 (middle)	12.8	9.5	14.6
	17.8	0.8	1.3
	20.3	0.8	1.5
	18.4	0.7	1.8
	18.1	0.7	1.4
	15.4	1.1	1.8
	15.1	7.2	14.9
	13.4	0.9	2.1
	13.4	0.8	1.9
	5.5	0.9	2.6
	13.8	0.9	1.7
	7.1	0.9	1.8
	4.1	1.9	3.0
1533 (downstream)	13.0	1.4	1.0
	18.4	1.2	0.9
	19.1	1.8	1.8
	17.5	2.1	2.1
	15.1	1.3	1.4
	14.5	1.9	1.9
	14.9	1.4	0.5
	5.6	1.6	0.8
	6.8	1.2	0.8
	4.4	1.9	1.3

The Flintham and Carling approach resulted in higher total shear stress values at only the upstream left bank. The rest of the banks show lower shear stress values using the Flintham and Carling approach. This result is to be expected, as the shear stress partitioning method does not predict the higher shear stresses that are generated at channel bends. After comparing the Einstein and Carling approaches with one another,

the shear stress values can be compared with the discharge to look for a relationship between the bank shear stress and the flow.

Shear Stresses and the Stream Flow

In order to also look for a relationship between the shear stress at the banks and discharge, the results for both shear stress methods were compared with the associated discharges for each flow (Figure 10, Figure 11).

(A)

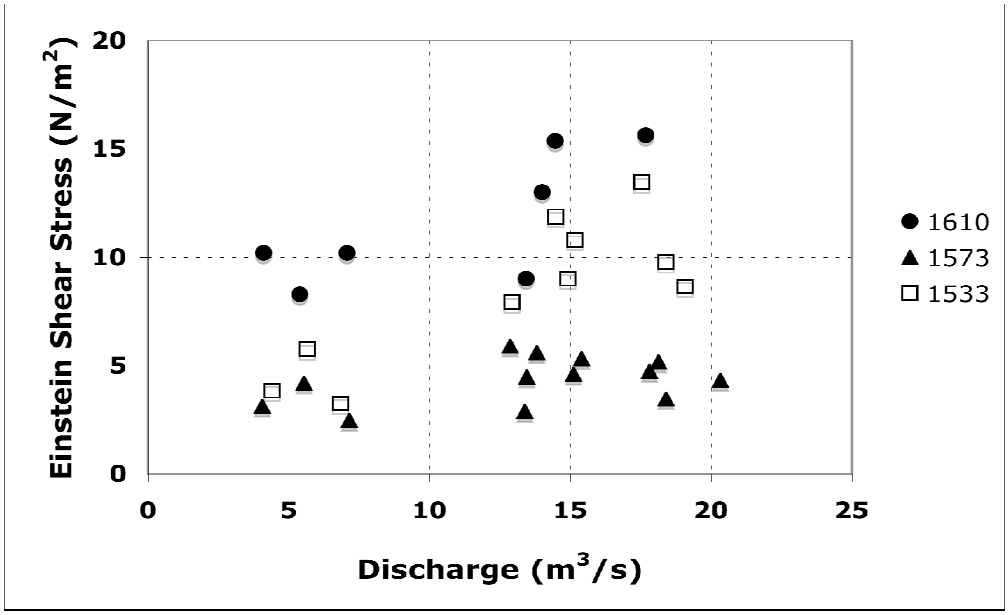

(B)

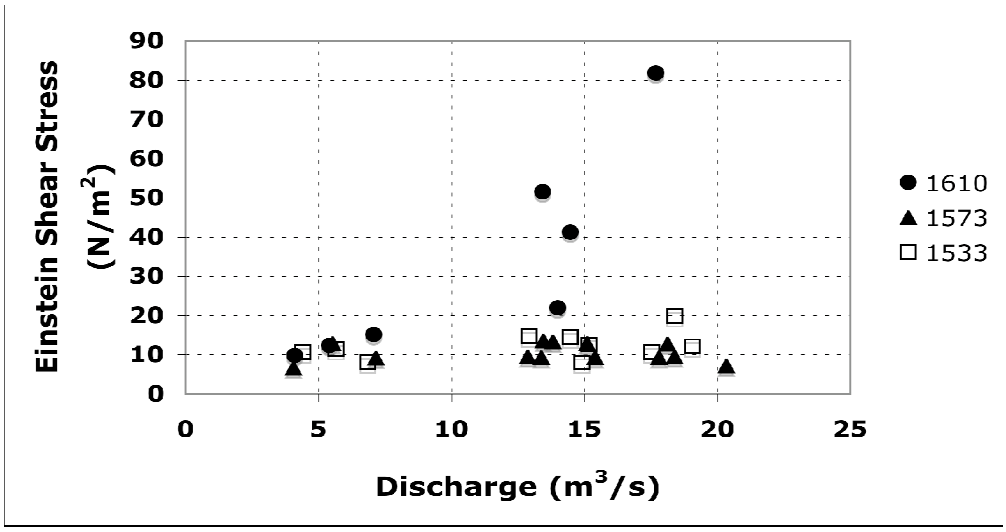

Figure 10: Comparisons of Einstein shear stress on the left (A) and right (B) banks. 1610 is the site closest to the meander bend with sites 1573 and 1533 further downstream, respectively.

(A)

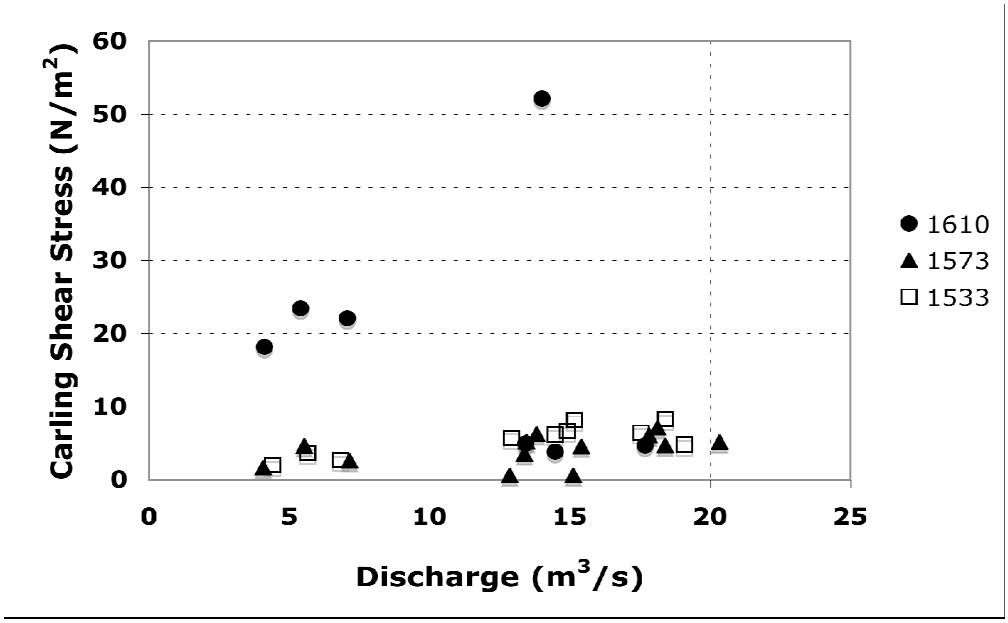

(B)

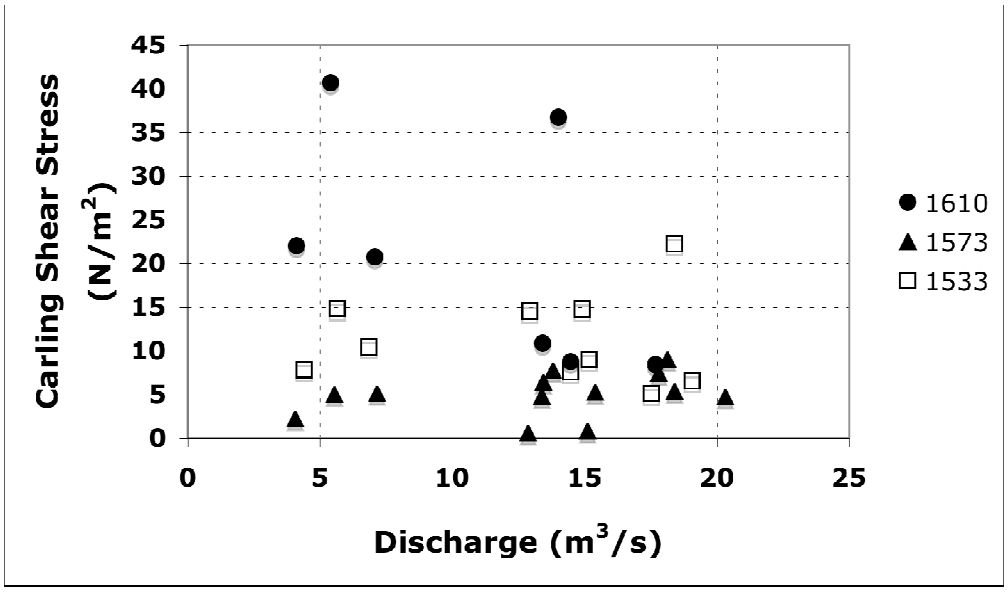

Figure 11: Comparisons the Carling shear stress on the left (A) and right (B) banks with discharge. 1610 is the site closest to the meander bend with sites 1573 and 1533 further downstream, respectively.

The Einstein shear stresses correlate linearly at all three sites on both banks with discharge. The same is true for the two further downstream sites on both banks for the Carling shear stresses. However, the Carling shear stresses for both banks at the upstream site do not show this correlation with the discharge, with several points showing far lower shear stress values than the rest of the upstream data.

Bank Erosion along the East Fork River

Bank erosion was determined for the East Fork River by comparing the channel planform from 1980 USDA air photo data with 2006 Air photo data (Figure 12). These data indicate that bank erosion only occurred at the channel bends, as suggested by the Nanson and Hickin (1983; 1986) model and consistent with the shear stress data that indicates much higher shear stresses at the channel bend than at other sites.

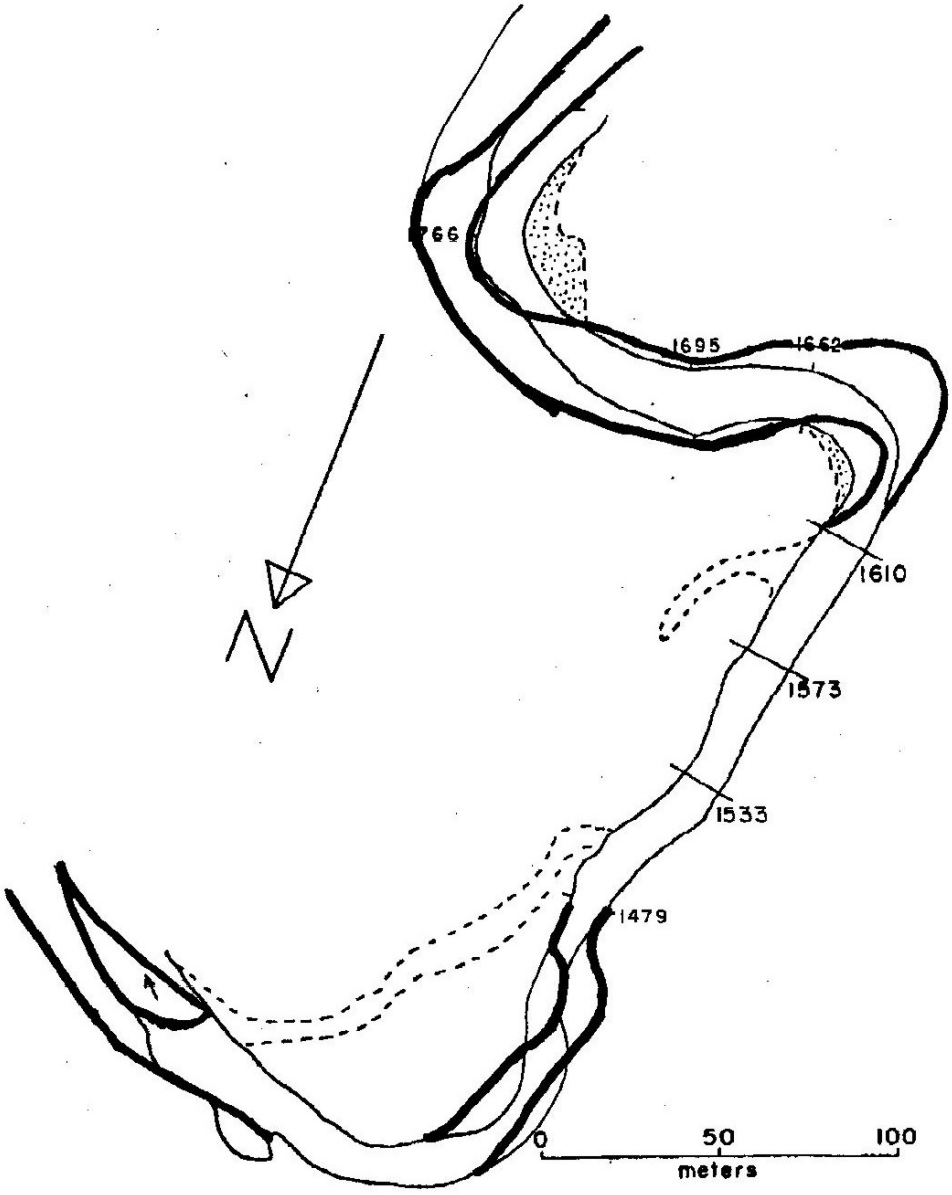

Figure 12: East Fork River channel planform from 1980 USDA air photo data with 2006 Air photo data in bold.

Discussion

In a very general way, both approaches predict that the shear stresses should be much higher near the bend than downstream of the bend, which would indicate higher rates of bank erosion near the bends. In detail, however, the data indicate that the alternative hypothesis is incorrect, and that curved river segments affect the shear stress distribution of nearby, straight reaches for a distance of over 100 meters downstream. The Flintham and Carling approach has been used in the field in previous studies (Julian and Torres, 2006) as a means for predicting the shear stress along the banks of a reach. Flintham and Carling (1988) stated that the approach should only be used on straight, trapezoidal reaches with homogeneous bank grain size. The section of the East Fork River used in this study is a straight section of reach, over 100 meters in length, with nearly trapezoidal channel morphology and homogeneous bank sediment with little to no bank roughness.

Therefore, the Flintham and Carling approach for calculating shear stress should yield values similar to the shear stresses measured using the Einstein method. However, the data shows that this is clearly not the case.

When the shear stress values for each method are compared in Figure 9, the data for each site on both banks do not show a one to one relationship. In fact, the trendlines for the upstream site show a negative slope. This is likely due to the upstream meander bend, which is around 20 meters upstream of the 1610 transect. The slopes for the sites change downstream and veer closer to 1, but even at site 1533, which is over 100 meters downstream of the bend, the meander still seems to influence the hydraulics along the banks. However, the shear stresses calculated from the Flintham and Carling approach

do decrease downstream from the meander bend, much like the shear stresses calculated from the Einstein-Barbarossa approach.

For nearly all of the sites, the Flintham and Carling approach yielded bank shear stress values less than those calculated from the total boundary shear stress. The only site that differed was the left bank at 1610. This is the bank outside of the meander bend. As a result, the water depth is higher due to the meander hydraulics. Because the Flintham and Carling approach does not incorporate the water surface gradient, it overpredicts the shear stress along this bank.

It is also the upstream 1610 site at which the Carling shear stresses do not correlate linearly with discharge. For both approaches at the two other sites as well as the Einstein approach at 1610, the shear stress values correlate linearly with the discharge. This further proves that although at 1610 the reach seems straight and is 20 meters downstream of the meander bend, a bank shear stress approach used for straight reaches cannot be used to accurately predict the shear stress. However, since the Flintham and Carling approach does yield shear stress values that decrease downstream of the bend and produces shear stress values that are not linearly correlated with discharge at the site just downstream of the meander bend, it is a fair predictor of where the bank hydraulics are affected by the upstream meander bend.

Conclusion

The purpose of this study was to investigate the methods for predicting shear stress along the banks of both straight and curved channels. The results clearly indicate that although the section of the East Fork River which was studied appears to be straight,

upstream morphology still influences the hydraulics along the banks up to 100 meters downstream. This is interesting as the meander wavelengths measured in Prestegaard (1982) imply that the stream should be interpreted as being straight with meander bends, the hydrologic data imply the opposite.

As a result, it is concluded that curved river segments affect the shear stress distribution of nearby, straight reaches. Therefore, using a shear stress prediction approach that assumes a reach to be straight on a section of river downstream of a meander bend likely will not yield accurate shear stress values. However, the same approach may still reveal the extent of a meander bend's influence on downstream bank hydraulics.

The East Fork River was an excellent site for this study because it is a simple channel with little to no bank roughness along the study reach. However, other regions in the United States contain streams that have more significant vegetation growing along their banks. These other streams are subject to hydraulic disturbances beyond channel curvature with the generation of macroturbulent eddies due to stream bank roughness elements.

Prediction of Macroturbulent Eddy Lengths from Bank Roughness Measurements

Introduction

Stream bank erosion provides a significant proportion of a stream sediment budget and it may be the main source of fine-grained sediment to downstream aquatic ecosystems (Eaton and Millar, 2004). Lawler (1995) identified three main processes of bank erosion that take place in different parts of the watershed. He suggests that fluvial entrainment is the prevailing mechanism of erosion in mid-basin reaches of watersheds. Stream banks in headwater areas have low bank shear stress, and tend to fail as bank ravel. In large watersheds, channel banks fail due to undercutting of the bank and mass movement processes. In the middle reaches of watersheds, the stability of banks is thought to be largely determined by the shear stresses acting on surficial bank particles. In this section, I will examine how bank roughness affects flow near the banks and bank erosion.

The roughness of a stream bank can affect the flow in two very different ways and result to either enhance or suppress bank erosion. Bank roughness can support resistance to flow, which lowers velocities and shear stresses near the bank. Bank roughness features of sufficient length, however, can generate macroturbulent eddies, which bring high velocity flow near the bank, enhancing bank erosion. Most research on bank roughness has emphasized the role of flow resistance in decreasing rates of bank erosion. Flow resistance of the bank alone, however is difficult to measure and it is often

determined by partitioning total resistance. Most flow resistance equations are derived by manipulations of von Karman's "law of the wall" that describes boundary layer flow:

$$V/u^* = u/(gRS)^{0.5} = 1/k \ln (Z/Zo)$$

where V is the average cross sectional velocity, $u^* = (gRS,)$ and Z is the height above the bed where velocity u is measured, and Zo is the height at which the logarithmic equation predicts a velocity of zero. Zo for logarithmic profiles is $1/30^{th}$ the roughness height. For most stream channels, data on roughness heights, Zo, and velocity profile measurements are not available. Therefore, simpler empirical expressions are usually used to define flow resistance based on simpler hydraulic variables. The dimensionless resistance parameter u/u^* is used to describe flow resistance in channels; the value of the parameter increases with smoother channels.

$$u/u^* = V/(gRS)^{0.5}$$

A frequently-used flow resistance equation similar to this expression is the Manning equation, which describes the relationships among flow depth, gradient, and boundary roughness. The expression below defines Manning's roughness coefficient, n, which increases in value with higher values of flow resistance.

$$\text{Manning's } n = (R^{2/3} S^{1/2})/V$$

where *V* is the average cross sectional velocity, *R* is the hydraulic radius *(A/P)*, *S* is the energy gradient and *n* is the Manning roughness coefficient.

Manning's roughness coefficient represents the total resistance to flow that originates from a variety of sources. Bathhurst (1993) subdivided the total resistance into three major components; free surface, channel, and boundary resistance. Free surface resistance represents the loss of energy resulting from hydraulic jumps, like surface waves, abrupt changes in water surface gradient, and macroturbulent eddies. Channel resistance is associated with undulations in the stream bed and banks and changes in channel form and cross-sectional shape. Channel and free surface resistance can account for half of the total resistance of a channel, however, boundary resistance, which results from the movement of water over grain roughness or microtopographic features in the bed or bank, has garnered the focus of most studies (Bathhurst, 1993; Ritter et al., 2002).

Despite the importance of boundary resistance in bank erosion processes, many studies incorporate bank roughness into a channel-averaged Manning's roughness coefficient. Bank roughness is often visually estimated to predict or model the influence of bank roughness elements on the flow dynamics of the stream (e.g. Dun, 2006; Nadan et al., 2006; Perumal et al., 2007). Many model and flume studies also use average roughness heights from the field as the basis for homogeneous roughness heights in the flume studies (e.g. Jarvela, 2002; Kouwen and Fathi-Moghadam, 2000; Wu, 2008).

In reality, however, bank hydraulics is influenced by a range of roughness heights, not just the average roughness height or an implied roughness coefficient from visual surveillance. The velocity profile near the stream bank depends on the height of

roughness elements. This dependence is related to the dynamic pressures exerted on the roughness elements. Dynamic pressures act on the sides of the roughness elements facing the flow, as well as their lee sides in association with flow separation, eddy formation, and shedding (Bridge, 2003).

Under conditions where the law of the wall is valid, larger bank roughness elements would generate larger *Zo* and larger resistance values, thereby increasing channel stability. Therefore, large roughness elements, whether rootwads or rip-rap, would generate a more stable channel. The assumptions are that an increased size in bank roughness would generate: a) greater resistance to flow, thus lowering near-bank velocities, and b) greater resistance to erosion, thus enhancing the stability of the features. In this research, I am proposing that isolated large roughness elements can generate macroturbulent eddies that promote erosion and that the critical size is related to the distribution of roughness lengths.

The purpose of this chapter is to investigate how size and spacing of roughness elements influence the formation of macroturbulent eddies that generate deviations from the law of the wall by bringing high velocity flow adjacent to the channel boundary, which can cause stream bank erosion. The hypotheses to be tested are:

1. The range of bank roughness sizes is more important than the average size in the prediction of macroturbulent eddies that might generate erosion:
    a. The number of bank protrusions in natural streams is inversely proportional to the size of the protrusions.
    b. The spacing between protrusions is proportional to the size of the protrusions.

c. There is an upper limit on size and spacing of bank protrusions in a given reach of river, which is scaled by the size of the features that generate the protrusions.

2. In a given reach and discharge, there is a critical protrusion size at which coherent macro-turbulent eddies are generated. This concept of a critical size is illustrated in Figure 13.

3. The null hypothesis is that protrusion size and eddy generation are not related, and therefore, eddy length scale and erosion rate are not proportional to protrusion size or spacing.

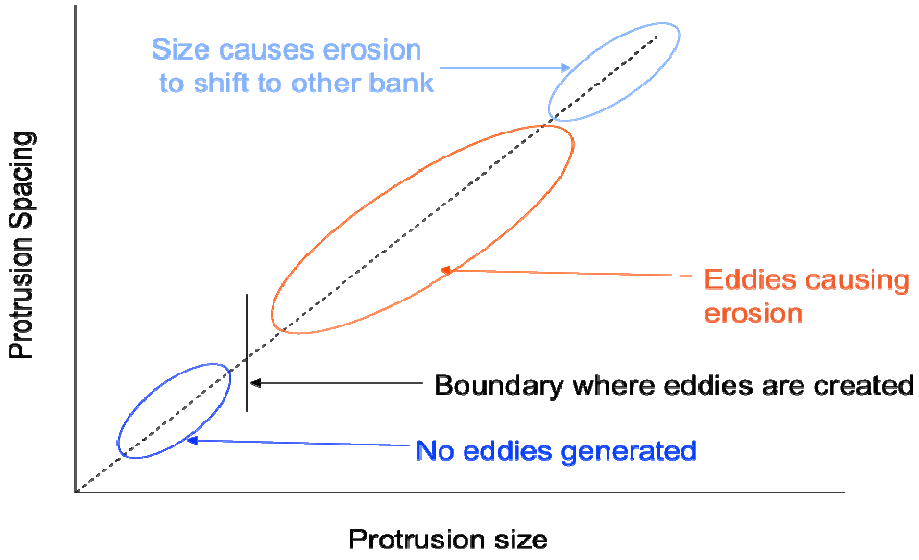

Figure 13: Logarithmic relationship between roughness size and roughness spacing.

Previous Research

Macroturbulent Eddies

In fully-developed turbulent flow, energy is dissipated by eddy formation. Meneveau and Sreenivasan (1987) adapted Kolmogorov's (1962) classical view of the eddy cascade in the inertial range to develop a simple model for the energy-cascading process in the inertial range that fits the entire spectrum of scaling exponents for the dissipation. Meneveau and Sreenivasan (1987) present a simplistic model in which an eddy of size r will break down into $2d$ eddies of equal size $r/2$, with d being the dimensionality of the space analyzed. A fraction $p1$ is distributed equally among one half of the new $2d$ eddies, while a fraction $p2 = 1 - p1$ is equally distributed among the other new eddies. This process is repeated with a fixed $p1$ until one reaches eddies of Kolmogorov length scale N. Figure 14 shows a one-dimensional version of the eddy cascade model.

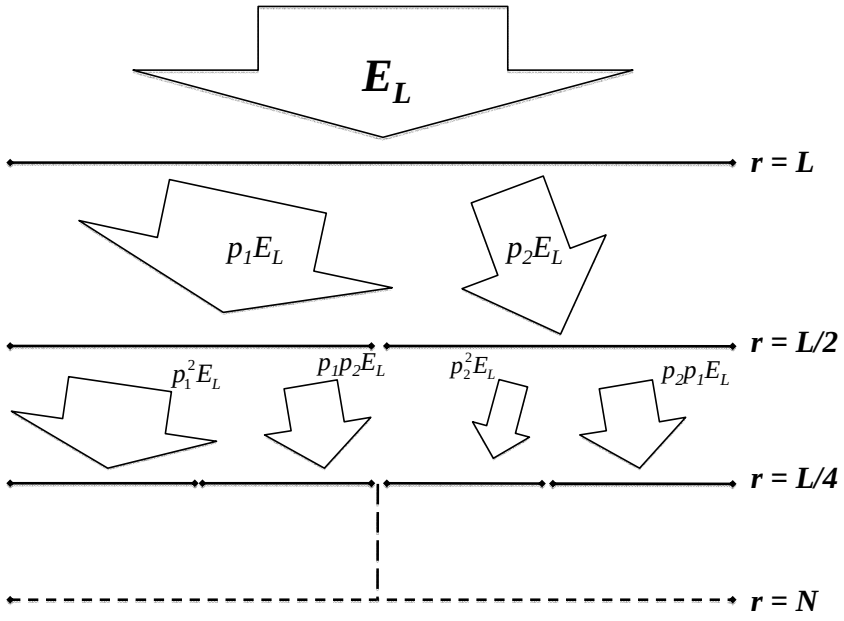

Figure 14: One-dimensional version of Meneveau and Sreenivasan's (1987) eddy cascade model with eddies breaking down into two new ones. L is the size of the initial eddy. E_L is the total dissipation in a domain of size L. The flux of kinetic energy to smaller scales is divided into nonequal fractions of p_1 and p_2. The eddy cascade terminates when the eddies are of the size of the Kolmogorov scale, N.

The Meneveau and Sreenivasan model describes the transfer of kinetic energy from a large eddy to smaller eddies, but it does predict the size of the largest macroturbulent eddies. In natural rivers, bank roughness is usually much larger than bed roughness (Hooke, 1980). High width to depth ratios in most rivers minimize the effects of bank roughness on total flow resistance, but macroturbulent eddies can generate effects that may have significant effects on river morphology. Macroturbulent eddies off the bank appear to be generated by bank protrusions or bank roughness. Therefore, large roughness elements will hide smaller roughness elements, and as a result, only the largest

roughness elements along a selected length scale will spawn macroturbulent eddies. This study attempts to build upon the eddy cascade model by examining the distribution of roughness heights and their relationship to macroturbulent eddies.

Field or laboratory documentation of the eddy cascade has been conducted primarily through the use of time series data on velocity that are evaluated using Fourier or wavelet analyses (e.g. Carrasco and Vionnet, 2004). In his analysis of time series velocity data near a bank-generated eddy in Paint Branch Creek, Houghton (1997) used Fourier analysis to determine macroturbulent eddy scales. His data indicated that the macroturbulent eddy length was two to three times larger than observed in the field.

Raupach (1992) developed a method (Figure 15) for predicting the sheltered area behind roughness elements in aeolian erosion. This method was then used by Sutton and Neuman (2008) to further observe the role of vortical structures shed by roughness elements in the initiation of sand entrainment and transport.

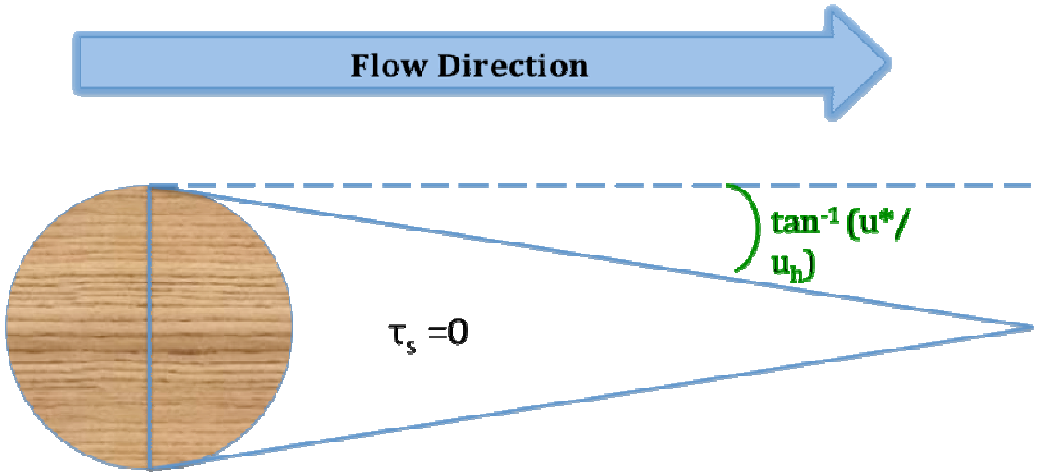

Figure 15: Raupach's (1992) effective shelter area for a roughness element. Where u^* is the shear velocity, u_h is the velocity at height h, and τ_s is the effective shear stress.

There have been a few studies that have examined the relationship of roughness heights with the generation of macroturbulent eddies and associated bank erosion (e.g. Bauer and Schmidt, 1993; Carter and Anderson, 2006; Abad et al., 2008). In most of these studies (e.g. Carter and Anderson, 2006; Abad et al., 2008), the focus of the research was bank erosion, and eddies were observed but not measured nor further discussed beyond the observations. Bauer and Schmidt (1993) studied flow patterns and morphologic adjustments of sandbars. They observed that recirculation eddies form on the lee side protrusions, sandbars and found that these eddies, when coupled with surface waves, could entrain sand and deposit it in the recirculation eddy. Abad et al. (2008) investigated how bendway weirs (protrusions at channel bends designed to minimize bank erosion) influence flow dynamics and stream bank erosion. At low flow, the authors found recirculation eddies formed at the weirs. Due to their low velocities at these gauges heights, the eddies deposited sediment, instead of eroding it.

There have been several studies of the effects of macroturbulent eddies on bedrock erosion. Carter and Anderson (2006) investigated the evolution of slot canyons and the influence of wall shapes on flow dynamics. They found high erosion rates in the back eddies on the lee side of wall bumps. The erosion caused by the back eddies created low-angle sharp cuspate edges out of the initial rounded sinusoidal wallforms. These features are similar to the lateral potholes formed in bedrock downstream of protrusions that have been described by Zen and Prestegaard (1994).

Macroturbulent eddies have been evaluated as bank erosion mechanisms only in unusual circumstances. The purpose of this research is to determine whether macroturbulent eddies are common features along vegetated stream banks, where roughness lengths are relatively large, and to determine whether erosion associated with macroturbulent eddies should be viewed as a common part of the bank erosion process.

Methods

Choice of Field sites

Three sites were chosen for this study. The criteria for site selection include: a) Moderately straight reach at least 50 meters in length, b) Variations in roughness spacing among the sites, c) Sites where bank erosion rates are known, d) Sites where depth and discharge are gauged, and thus mean velocity can be calculated and average boundary shear stress can be determined if water surface gradients are measured. Using these criteria the following reaches of river were chosen in the Anacostia River system (Figure 16, Table 5).

a) **Northwest Branch of the Anacostia at the 38th Street Bridge**, (near USGS gauge) is an engineered channel, trapezoidal in shape with large homogenous rock rip-rap lining the banks. The rock roughness has a normal probability distribution. Maintenance of the engineered channel has prevented the growth of shrubs or trees, therefore, large roughness heights are generated by the rip-rap itself. This site is engineered to have a bank erosion rate of zero.

b**) Little Paint Branch at Greencastle Road** is located in the upper reaches of Little Paint Branch Creek. The bank height is low, while bank roughness is high and consists of closely spaced oak trees of similar size, which gives the appearance of homogeneous vegetation roughness. The stream occupies a wide riparian corridor. A Global Water WL16 Level Logger has been installed at the site to measure gage height as a function of time.

c**) Little Paint Branch at Cherry Hill Park** is located approximately 6 km downstream from the Greencastle Road site. The channel is about 3 times wider than the Greencastle site. The site has large erosive areas along the banks and long-term bank erosion rates are known for this site (Behrns, 2007). Roughness is generated by tree trunks, rootwads, roots, and other features over a range of spatial scales. A Hach MS5 Multimeter has been installed at the site to measure gage height, conductivity, and turbidity.

38th St. Bridge **Greencastle Rd.** **Cherry Hill Park**

Figure 16: Photographs of the three research sites, 38th Street Bridge, Greencastle Road, and Cherry Hill Park.

Table 5: Description of the three sites. τ_o is the bankfull total boundary shear stress, and τ_{bank} is the bankfull shear stress on the bank, determined using the Flintham and Carling (1988) approach (see previous chapter).

Site	Position in Watershed	Channel Type	Width/Depth	τ_o (N/m^2)	τ_{bank} (N/m^2)	Bank Roughness
38th Street Bridge	Downstream, near mouth	Engineered, trapezoidal channel	8.3	120	53	Rock Homogeneously sized
Greencastle Road	Upstream near headwaters	Natural	15.3	9.0	12	Trees, spaced homogeneously
Cherry Hill Park	Mid-watershed	Natural	14.5	41	20	Heterogeneous material and spacing

Field Measurements

Measurements used in this investigation to compare roughness heights to eddy length scales at a variety of gauge heights included (1) topographic surveys of bank morphology and roughness heights, (2) water surface gradients for a variety of flows, (3)

roughness size of protrusions at various flows, and (4) eddy lengths on the lee side of protrusions.

Bank morphology/roughness height measurement methods were developed separately for trapezoidal banks and near-vertical banks. Roughness heights at trapezoidal banks were measured by measuring the bank every five centimeters along a line level from the bank to the line (Figure 17A). Bank morphology of near-vertical banks was measured using a Leica Disto A3 laser distance meter along a fixed path in the channel. Measurements from the path to the bank were taken at least every meter (Figure 17B).

(A)

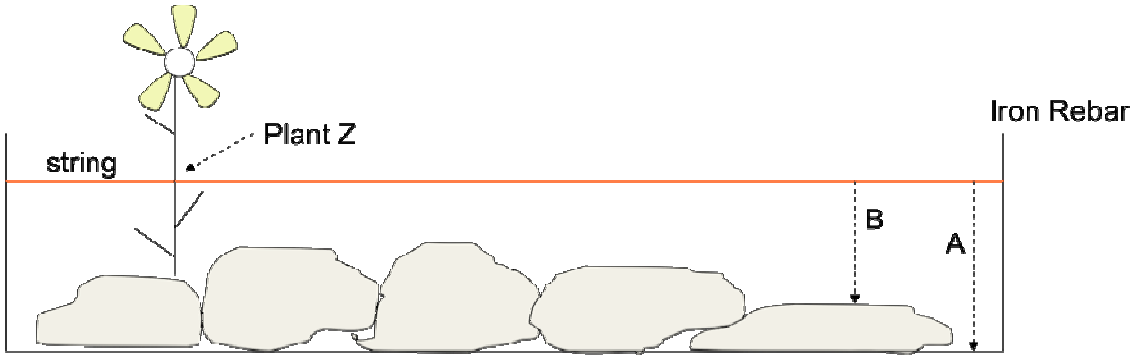

Actual rock Ks = A - B

Actual veg. Ks = actual rock Ks + Plant Z

(B)

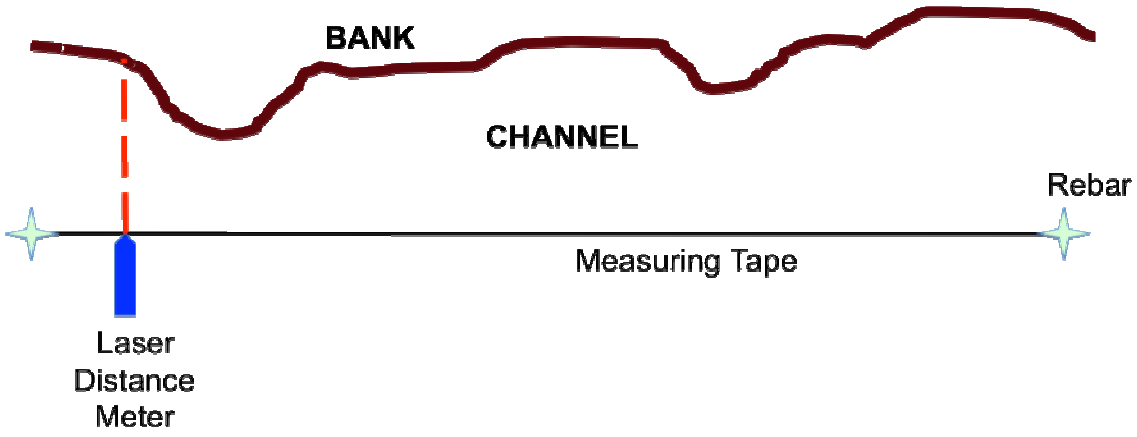

Figure 17: Schematics for measuring bank morphology/roughness heights for trapezoidal banks (A) and near-vertical banks (B). (A) is a side view, and (B) is a plan view.

During storm events, the water surface was marked using flags and a carpenter's pencil. The length of macroturbulent eddies was measured during high flows using small floating particles to map the surface vortex. The eddy length was then measured using T-squares and meter sticks to an accuracy of several cm. Eddies length scales can be measured using electromagnetic or acoustic Doppler current meters (e.g. Houghton, 1997). These measurements are hard to relate directly to bank roughness features, and there is a suggestion that the method overestimates maximum macroturbulent eddy length (Houghton, 1997).

After the water receded, the bank profile/roughness, K_s, for that particular flow was measured using the laser distance meter along a fixed flow path with roughness readings taken at least every ten centimeters. All roughness data were analyzed to generate probability distributions of roughness heights and spacing of large roughness elements (Figure 18). These data were used to obtain average and standard deviation

(D84) values for roughness heights; values that are traditionally used to identify Ks for bank roughness. In addition, the roughness height data were plotted against the cumulative number of particles and roughness spacing to determine the portion of the distribution that are “fractal” and thus are embedded within the roughness cascade. This procedure was used to identify roughness heights that were significantly larger or more isolated than the adjacent roughness heights.

(A)

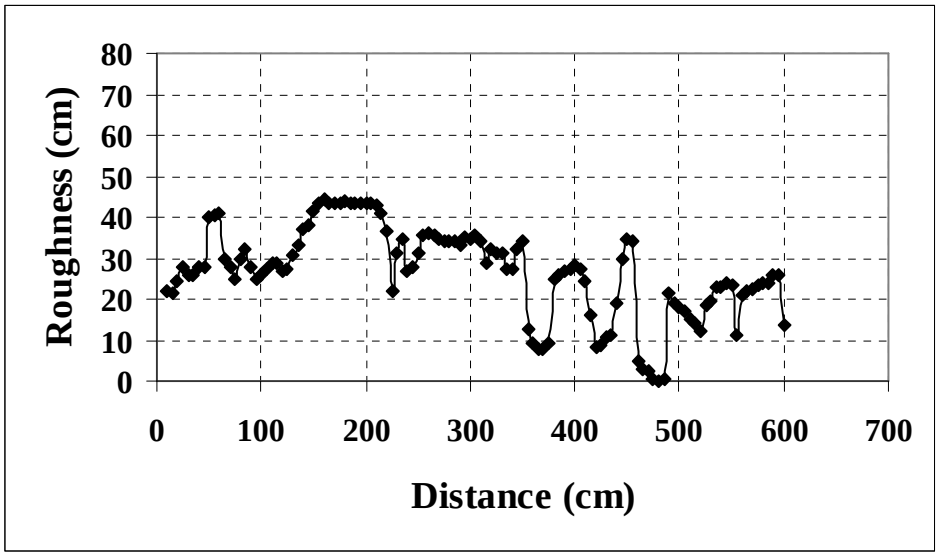

(B)

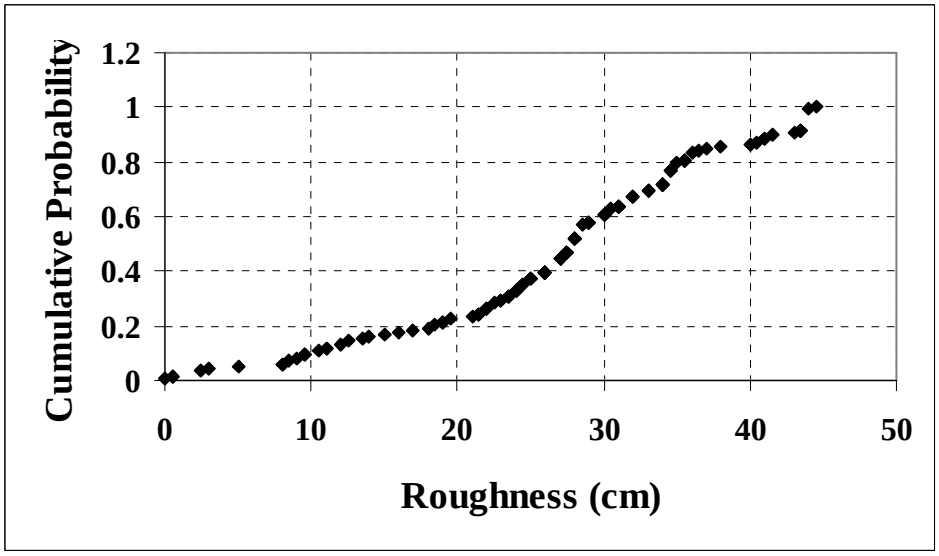

Figure 18: (A) Example of rock roughness heights measured along the trapezoidal channel. (B) Cumulative probability distribution of the roughness heights. Hydraulic roughness often correlates with the 84th percentile of roughness; this relationship is derived for bed particle roughness and applied to bank roughness heights.

Eddy Length Prediction

In this paper, I will compare the field measurements of eddy length for various flows with eddy lengths predicted from Raupach (1992), who developed a method to predict the shelter area for isolated roughness elements. Raupach characterized the wake of an isolated surface roughness element in terms of an effective shelter area *A*, which describes the reduction of substrate surface shear stress τ_S in the roughness element's wake. The area can be defined as the area integral of the normalized substrate surface stress deficit:

$$A = \iint \left(1 - \frac{\tau_S(x,y)}{\tau_{S0}}\right) dxdy$$

where $\tau_S(x,y)$ is the shear stress at point (x,y) and τ_{S0} is the unsheltered substrate surface shear stress in the same wind conditions, equal to $\tau_S(x,y)$ far from the isolated roughness element. A is the area within which the substrate shear stress must be set to zero in order to produce the same integrated stress deficit as that induced by the roughness element.

In developing this method, Raupach provided the means to predict eddy length associated with a roughness element when given the roughness height, shear velocity, and velocity at height of the roughness element. This method was then adapted to be used to calculate the predicted surface eddy length for a protrusion (Figure 19). The predicted eddy length is obtained by:

$$\tan^{-1}(u^*/u_h) = \theta$$

$$EL = K_s/\tan\theta$$

where u^* is the shear velocity, $(gdS)^{0.5}$, g is the acceleration due to gravity, d is flow depth, S is the water surface gradient, u_h is the surface velocity, θ is eddy's angle of entry towards the bank, K_s is the roughness height, and EL is the predicted eddy length.

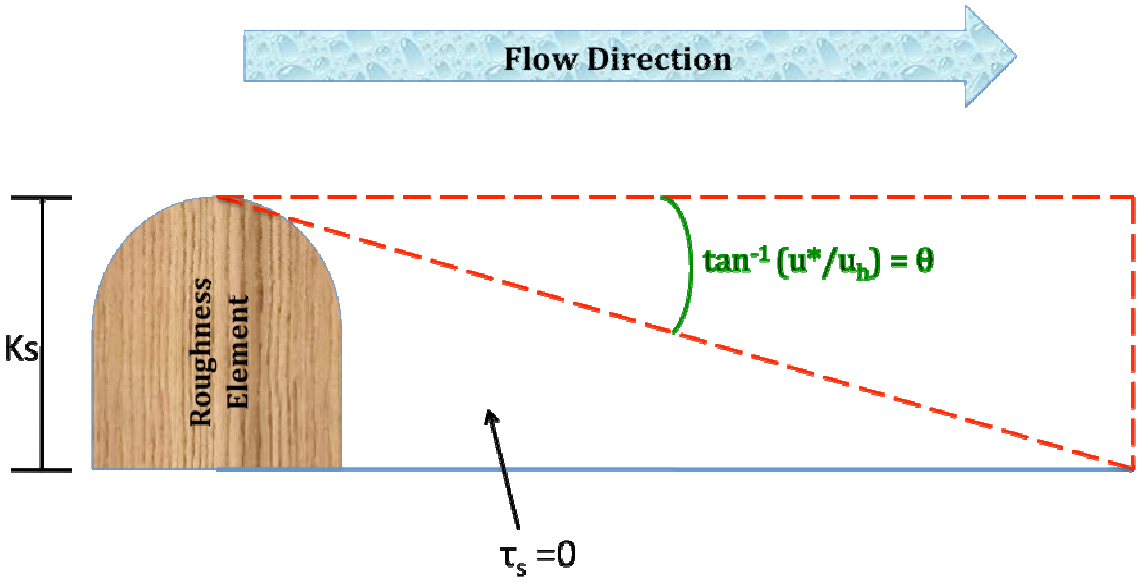

Figure 19: Adaptation of Raupach (1992) to predict surface macroturbulent eddy length. The predicted eddy length, *EL*, is equal to the roughness height divided by the tangent of theta.

Results

Bank Roughness

Three reaches were examined: the NW Branch at the 38th St. Bridge, Greencastle Road, and Cherry Hill Park. The NW Branch site is an engineered, trapezoidal channel with rip-rap lining the bank and was measured from baseflow to the approximate 50-year flood level, with the bankfull flow located within the channel. Because the site is engineered and trapezoidal, bank protrusions could be measured along the entire height of the bank. This is not the case with the other two sites. The Greencastle Road and Cherry Hill Park sites are more vertical. All of the large roughness elements on their banks reside along the approximate bankfull stage. As a result, the roughness sizes at these two sites were measured only along the bankfull flow height. The Greencastle

Road site has banks lined predominantly by trees. The Cherry Hill Park site has banks made up of mostly tree roots and rootwads. Although all banks were defined as being straight prior to data being collected, field measurements show otherwise. The banks exhibit a variety of roughness heights (Figure 20), even at the NW Branch site, which was defined as having homogeneous bank roughness.

(A)

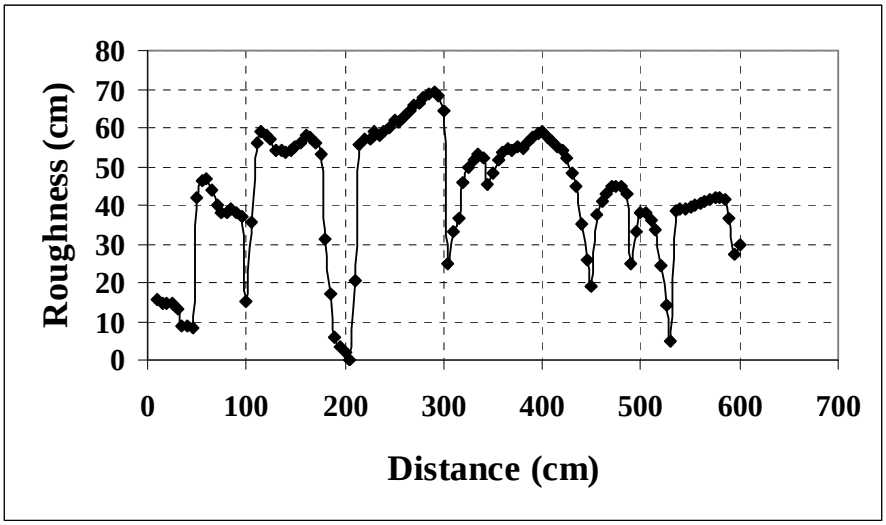

(B)

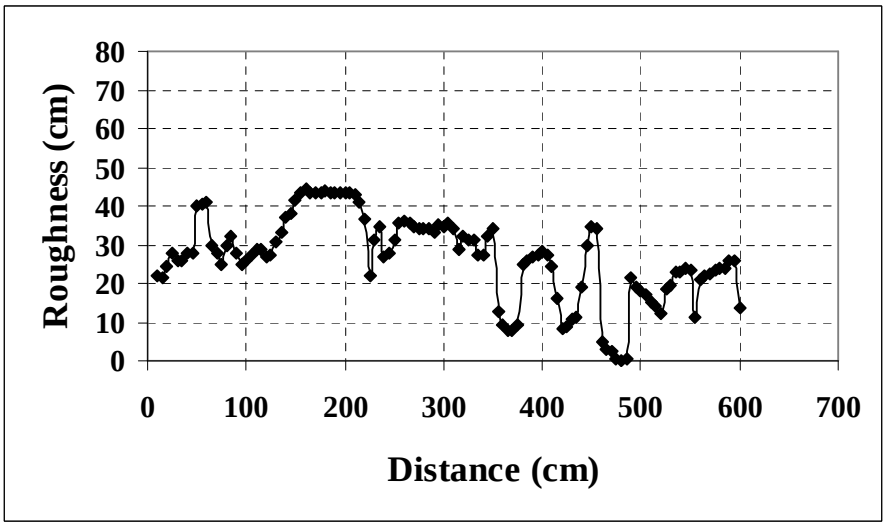

(C)

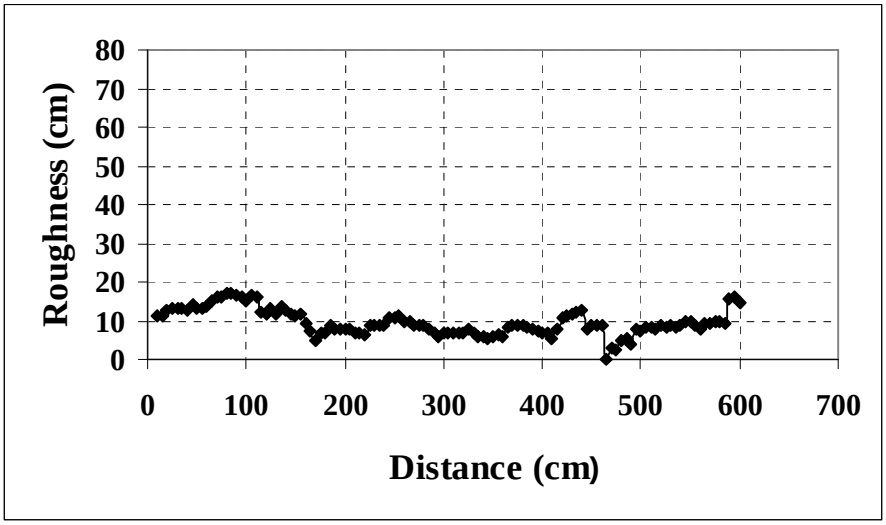
Roughness (cm)
80
70
60
50
40
30
20
10
0
0
100
200
300
400
500
600
700
Distance (cm)

(D)

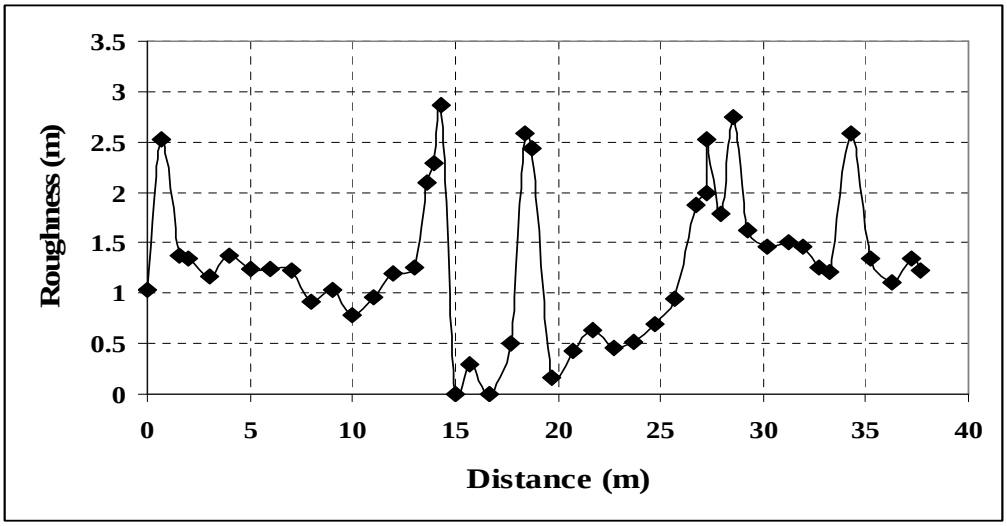
Roughness (m)
3.5
3
2.5
2
1.5
1
0.5
0
0
5
10
15
20
25
30
35
40
Distance (m)

(E)

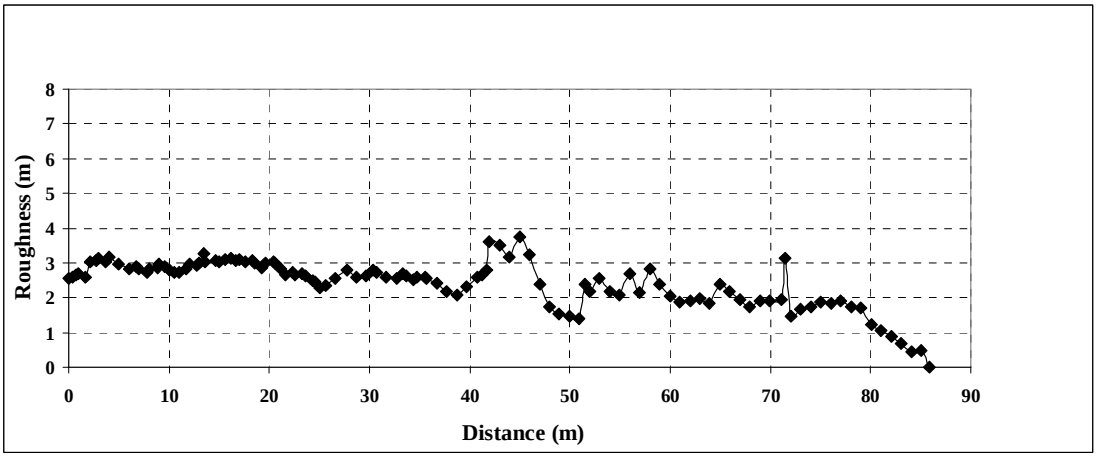

Figure 20: Bank morphology measurements of 38th St. Bridge at baseflow (A), 3 meters up the bank (B), and 6 meters up the bank (C), Greencastle at bankfull flow (D), and Cherry Hill at bankfull flow (E). Measurement error was less than the size of the points on the graphs.

Roughness heights at Northwest Branch are generated by large boulders of a similar size range (rip-rap). The roughness heights generated by these particles vary as a function of the position on the bank. Maximum roughness heights and spacing are limited by the size of the boulders. The maximum roughness height found at this site was 69 cm. Table 6 shows the average and D84 roughness heights. The morphology flattens out up the bank. In addition, the roughness heights decrease in size by approximately one half from the baseflow to 3 meters up the bank, to 6 meters up the bank. The spacing between the large roughness heights is quite small as they are less than the maximum roughness height. The tight spacing of roughness elements helps protect the bank and prevents macroturbulent eddies from eroding significant sediment from between the boulders. Using the Raupach equation, maximum macroturbulent eddies generated along

these banks would have length scales of 30-60 cm. These could be observed, but not measured in the field due to that lack of stationarity (which also makes them less effective as erosion mechanisms).

Maximum Roughness heights at Greencastle are generated by tree trunks, while the minimum roughness heights are generated by grain particles. The tree trunks are fairly similar is size. The tree trunks range is size from around 2.5 meters to nearly 3 meters over the 38 meter-long reach.

Maximum roughness heights at Cherry Hill Park are generated by rootwads. The minimum roughness heights are, like Greencastle, generated by grain particles. The rootwads are heterogeneously sized and spaced. There is approximately a two-meter size difference between rootwads. The spacing between rootwads varies from around 5 meters to approximately 20 meters in length.

Table 6: Summary of roughness sizes at the sites. *St.Dev.* is the standard deviation for the roughness sizes. *Zo* is estimated to be $1/30^{th}$ of the mean roughness size, *D50*.

Site	D50 (cm)	D84 (cm)	St. Dev. (cm)	Zo (cm)
NW Branch				
Baseflow	42.7	58.4	16.9	1.4
3m Up	26.7	37.4	10.9	0.9
6m Up	9.6	13.9	3.3	0.3
Greencastle	133.3	240.2	73.8	4.4
Cherry Hill	245.4	313.3	66.2	8.2

However, bank roughness heights alone do not provide enough information to interpret macroturbulent eddies. The number and spacing of large roughness elements must be analyzed in order to see what roughness heights fall above the roughness cascade. These roughness heights are likely to cause macroturbulent eddies. At a site

where numerous roughness elements fall off of the roughness cascade, even average or D84 roughness heights may generate macroturbulent eddies.

Number and Spacing of Bank Roughness Heights

After measuring all of the roughness heights along a reach, it is possible to analyze the number of large roughness elements and their spacing. This allows for the identification of roughness heights that within each distribution might be large enough and isolated enough to generate eddies. The number (Figure 21) and spacing of roughness elements follows a power law (fractal distribution) for only part of the range. Large particles that are widely spaced, and thus fall off the roughness cascade, are found at all locations.

(A)

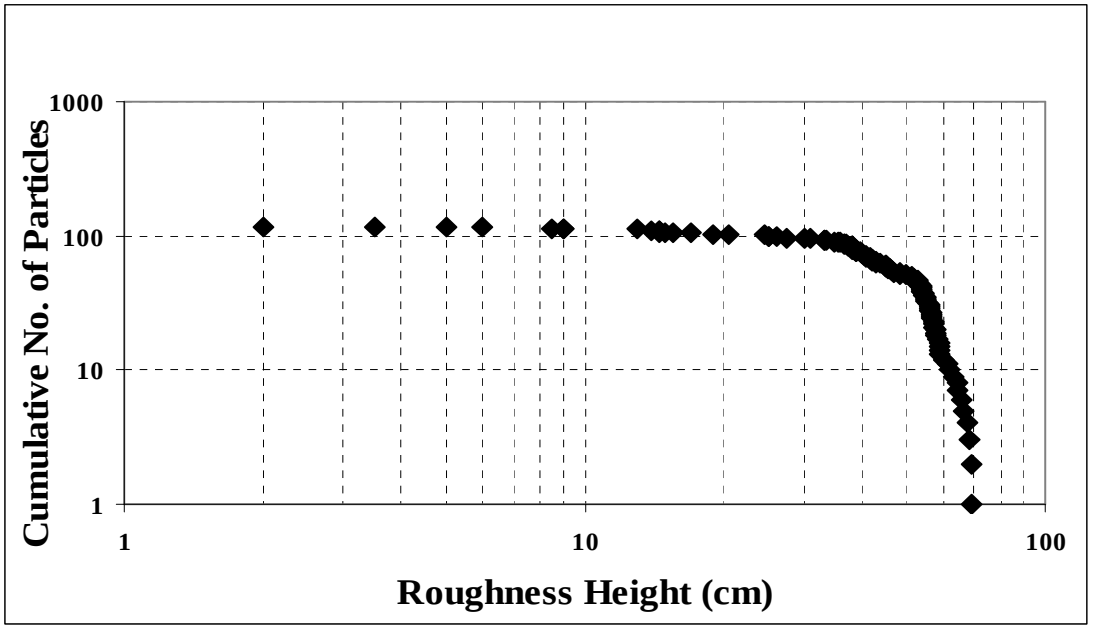

(B)

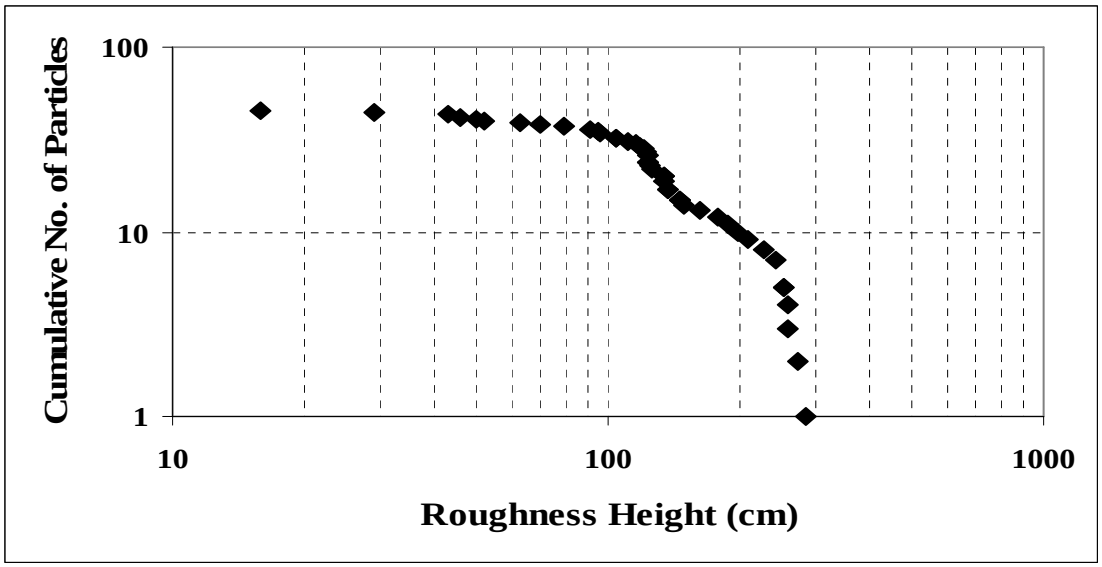

(C)

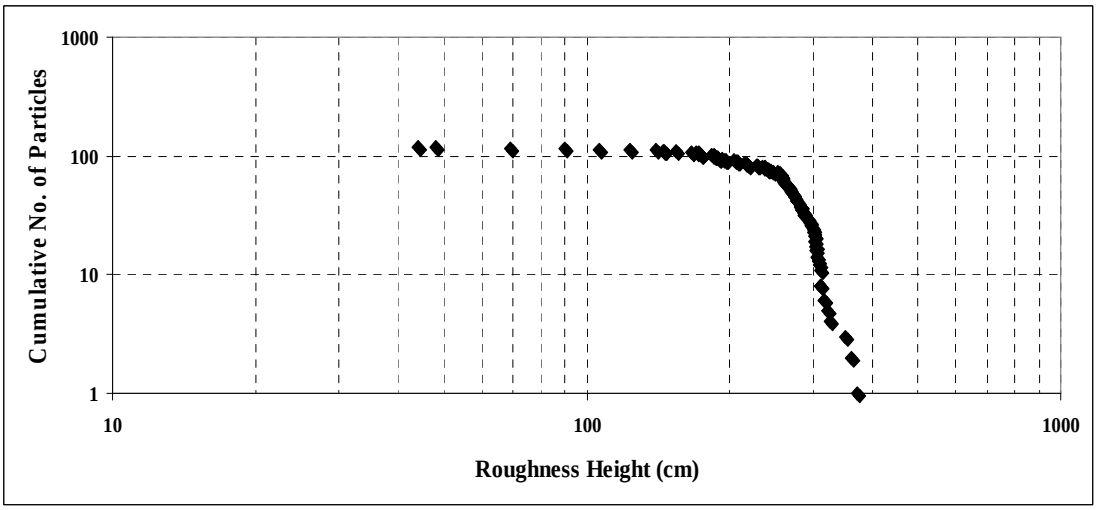

Figure 21: Cumulative number of particles and roughness heights for the baseflow of the NW Branch at 38th St. Bridge (A), bankfull flow at Greencastle (B), and bankfull flow at Cherry Hill (C).

The spacing data can be used to define upper and lower bounds for the fractal distribution of these parameters (Figure 22). Large roughness elements that are isolated

are more likely to generate macroturbulent eddies. Therefore, sites with more large roughness elements that fall above the roughness cascade will have a greater occurrence of large eddies that fall above the eddy cascade. Thus, these sites will have a larger occurrence of macroturbulent eddies.

(A)

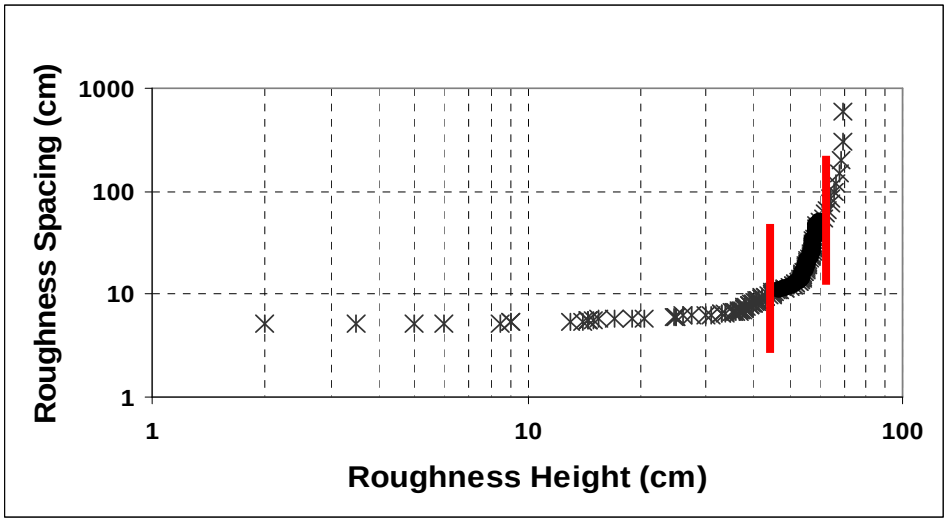

(B)

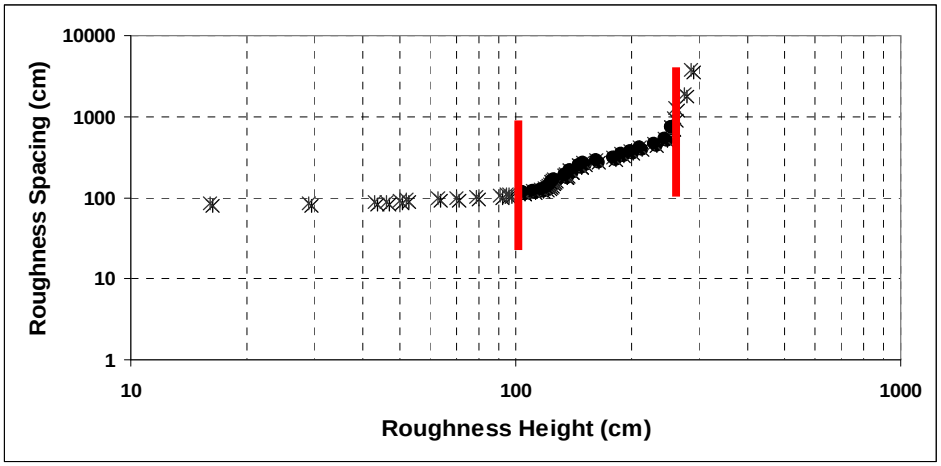

(C)

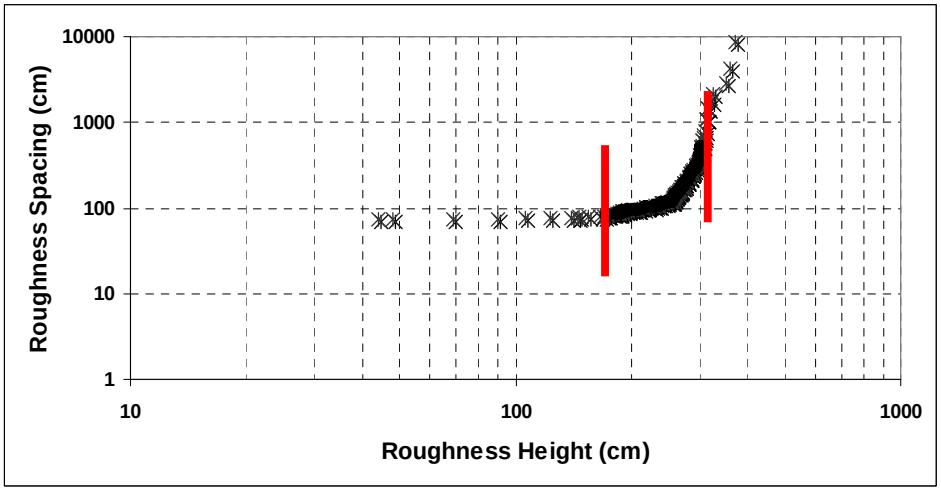

Figure 22: Roughness spacing for the baseflow of the site with rip-rap-lined banks (A), bankfull flow at the tree trunk roughness site (B), and bankfull flow at the rootwad

roughness site (C). Dark circles indicate points along the roughness cascade. Crosses indicate points the fall above or below the roughness cascade. The red lines indicate the upper and lower bounds of the roughness cascade.

Upper boundaries on the spacing are: particle size (NW branch) and vegetated bank length (controlled by alternate bar spacing in the two other reaches). The rip-rap at the NW Branch site has much smaller roughness heights. The maximum *Ks* is the size of the boulders. At Greencastle, the maximum *Ks* is the size of the tree trunks from the trees lining the banks. The tree trunks are fairly homogeneous in size (see Figure 20D). The maximum *Ks* at Cherry Hill is the size of the rootwads, both living and dead. The rootwads are the largest roughness elements of the three sites. It is difficult to define the exact roughness cascade at the rootwad site. It even appears as though there are two entirely separate roughness cascades. Even if this was the case, there are a number of roughness elements whose size and spacing still falls off the cascade.

The roughness heights at the sites that do fall off the cascade are potential sites for the generation of stable, macroturbulent eddies. These eddies, once generated, can be measured in length and compared to both the roughness height and flow conditions.

Roughness Heights and the Generation of Macroturbulent Eddies

Macroturbulent eddy lengths were measured during storm events at both the Cherry Hill and Greencastle sites over several months in 2008 and 2009. In order to try understand what governs the length of the eddies, it is necessary to identify both the roughness and flow conditions under which they form. Table 7 shows the range of eddy

lengths for protrusions at the two sites. Some of the roughness heights at each site that generated macroturbulent eddies were less than the average roughness size for the site.

Table 7: Eddy lengths measured at Cherry Hill (CH) and Greencastle (GC) and associated Reynold's numbers.

Storm Date	**Site**	**Roughness Height (m)**	**Eddy Length (m)**	**Reynold's Number**
11/13/08	CH	0.69	1.6	$1.57x10^6$
1/7/09	CH	0.74	2.1	$1.94x10^6$
1/7/09	GC	0.85	4.5	$3.37x10^5$
4/3/09	GC	2.15	2.0	$1.25x10^6$
4/3/09	CH	0.83	1.4	$1.53x10^6$
4/20/09	CH	0.94	2.6	$1.93x10^6$
4/21/09	CH	1.63	5.2	$3.42x10^5$
5/26/09	GC	1.86	3.2	$1.08x10^6$

In addition to physically measuring the macroturbulent eddy lengths, the eddy lengths were predicted using the Raupach method for the measured flow data. These predicted lengths were then compared to the actual measured surface eddy lengths (Figure 23). There is some correlation between the predicted and measured eddy lengths, with the predicted eddy lengths being two to three times larger than the measured eddies.

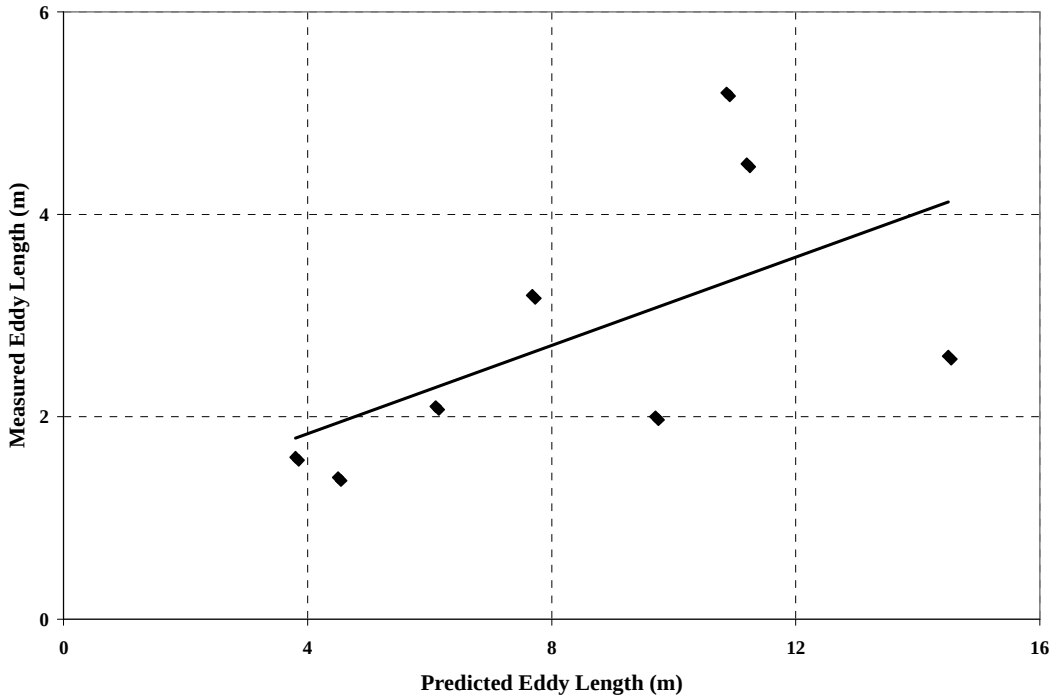

Figure 23: A comparison of measured eddy lengths and predicted eddy lengths. Predicted eddy lengths were two to three times larger than the measured eddy lengths. The trendline equation is $y = 0.2182x + 0.9604$ with an R^2 equal to 0.3378.

There is a range of measured and predicted eddy lengths with roughness heights (Figure 24). Although there is no clear correlation between either measured or predicted eddy length and roughness height, both comparisons appear similar in the shape of their distribution.

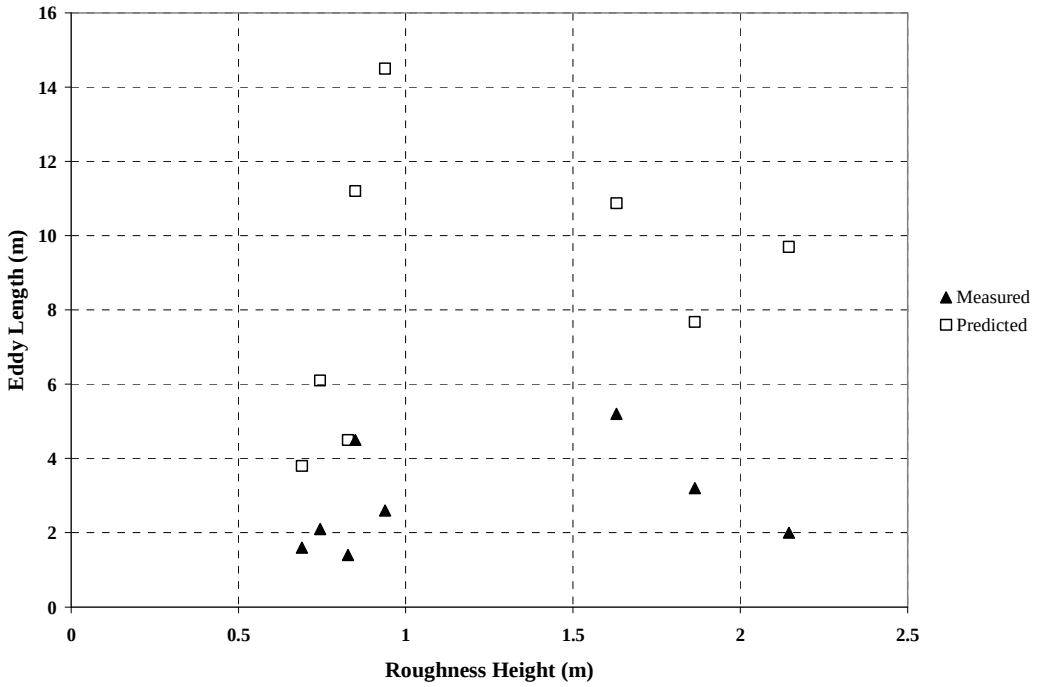

Figure 24: Measured and predicted eddy lengths (m) and their corresponding roughness heights.

Because the macroturbulent eddies are formed under bankfull conditions, the Reynold's number can be used as a control. The Reynold's number was calculated for each flow using

$$Re = (\rho dV)/\upsilon$$

where ρ is the fluid density, d is the mean depth, V is the mean velocity, and υ is the dynamic viscosity. The eddy lengths and Reynold's number are plotted in Figure 25. There appears to be a range of eddy lengths that occur at high Reynold's numbers (greater than $1x10^5$), but a possible lower limit of Reynold's number to the formation of

macroturbulent eddies. This is likely related to the flow depths needed to reach the parts of the bank with significant bank protrusions.

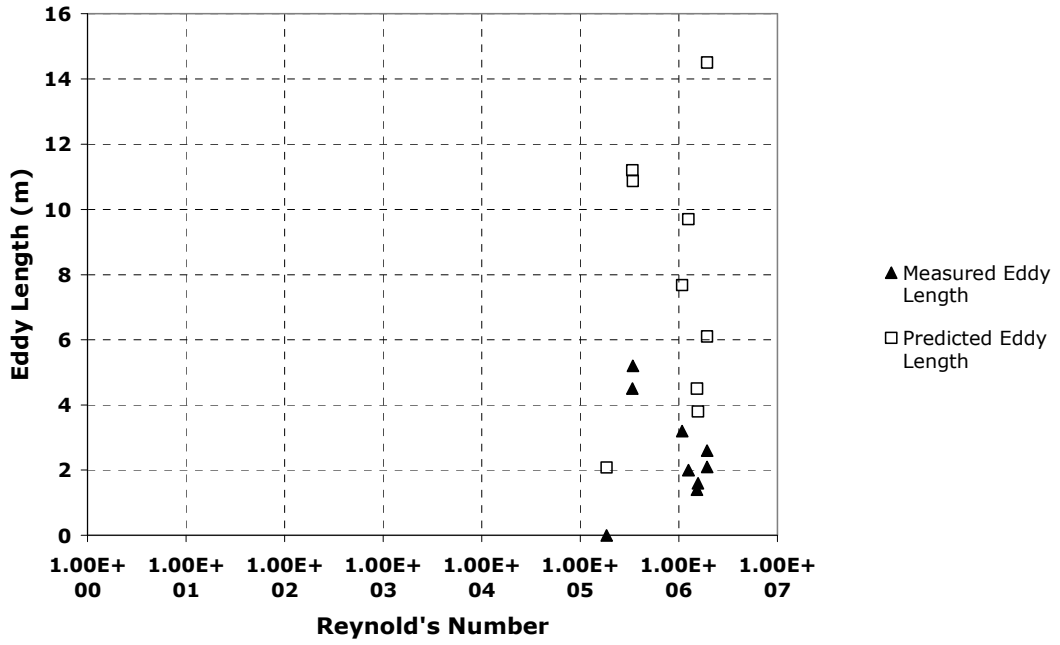

Figure 25: A comparison of measured and predicted eddy length with Reynold's number.

Discussion

The purpose of this study was to determine whether the size and spacing of large roughness elements along streambanks with typical bank vegetation are sufficient to generate macroturbulent eddies, and thus contribute to bank erosion. Numerous studies use average roughness height or a predicted Manning's roughness coefficient when calculating shear stress on the banks to predict or monitor stream bank erosion.

In the original hypothesis, it was proposed that there was an inverse power function relationship between the number of roughness elements and their size and a direct power function relationship between the spacing of roughness elements and their

size (Figure 13). In reality, however, there are constraints on both the number of particles and their spacing.

At the engineered, trapezoidal site, the spacing constraint is particle size, while at tree trunk-dominated and rootwad-dominated sites, the spacing constraint is the vegetated bank length. The vegetated bank length is controlled by the alternate bar spacing. For the tree trunk-dominated site, the alternate bar spacing is approximately 50 meters, and at the rootwad-dominated site the spacing is nearly 100 meters.

Although smaller than the tree trunks at Greencastle or the rootwads at Cherry Hill, some of the boulders at the NW Branch site are larger and isolated from the rest of the roughness elements. As a result, these boulders do generate eddies. The eddies scour the sediment between the rip-rap. This scouring can be seen by comparing the baseflow bank profile and the bank profile six meters up from baseflow. (Figures 20A and 20C). The boulders are homogeneous in size. The difference in *Ks* occurs because the baseflow bank height interacts much more with the flow, and therefore, experiences more erosion. Further up the bank, plants are able to grow in the sediment that is deposited between boulders, further smoothening the bank.

The data for the tree trunk-dominated reach show that not many small particles were measured. This is possibly due to the trees shielding or hiding the small roughness particles. However, the closely spaced tree trunks create a distribution of the large roughness sizes that don't fall off the fractal trend like the other sites do. This lack of isolated large roughness elements suggests that eddies are not likely to form at Greencastle, even though roughness heights are large. This may be the reason why we

see grasses growing on the banks at the Greencastle Road site. The banks are shielded from erosion and grass seedlings are able to sprout.

The third site has tree root roughness as opposed to rip-rap or tree trunk roughness. This does not hide small particles as effectively as the trees at Greencastle Road. The large particles are more isolated, and isolated roughness elements can be observed on the spacing distribution diagrams. The large, isolated particles are able to spawn macroturbulent eddies that also fall off the eddy cascade, and therefore, may elongate and reattach to the banks, where they cause erosion. This may be why we see little vegetation growing on the banks along this reach. Seedlings cannot grow because they are eroded away along with the bank substrate. Figure 26 is a picture at the Cherry Hill Park site taken after a large storm. The results of bank erosion can be seen to the right of the rootwad on the left-side of the picture.

Figure 26: Photo of bank erosion at the Cherry Hill Park site taken after a large storm. The stream flows from left to right. Significant bank erosion can be seen on the lee-side of the rootwad on the left-side of the photo.

Eddy lengths were predicted for the measured roughness heights at protrusions during storms. The predicted lengths were then compared with the measured eddy lengths from the same protrusions at the same flows. Although the two are positively correlated (Figure 23), the predicted eddy lengths are all two to three times larger than the measured eddy lengths. This difference may be due to the design of the Raupach (1992) wind tunnel scenario and the natural world. Raupach developed his method from predicting the sheltered area behind roughness elements by using isolated roughness elements. Yet, in the natural fluvial system, there is a range of roughness elements along a bank (Figure 20). As the eddy sheds off of the protrusion, it encounters other, smaller

roughness elements as it turns towards the bank. In addition, the Raupach equation includes the shear velocity, which is depth-dependent. Because banks are sloped, the eddy flows over shallower gauge heights as it turns towards the bank. This in conjunction with the addition of lee-side roughness elements is likely the cause of the actual eddies being shorter than the predicted eddy lengths. It is interesting, however, that the eddy length scales predicted from Fourier analysis of velocity data also generated much larger length scales than those observed with flow visualization in the field (Houghton, 1997). This suggests that interference of eddies with one another may result in shorter eddy lengths than would be obtained from isolated features.

The results of this investigation show that macroturbulent eddies can be generated along natural stream banks with no obvious protrusions; and that these eddies are common features along some streambanks (such as tree-lined banks) at high flows. Although there is no simple relationship between roughness height and eddy length (Table 7, Figure 24), larger, isolated roughness elements tend to lead to longer eddy lengths. It is interesting that both the Raupach (1992) method and field measurements of turbulence (Houghton, 1997) indicated longer length scales than actually observed. This suggests that interference among eddies may be a limiting factor in their lengths. There are numerous other factors involved in eddy creation and scaling in addition to roughness height. Flow depth, water surface gradient, and surface velocity also appear to influence eddy length as seen in the adaptation of the Raupach (1992) equation.

The results appear to show that at high Reynold's numbers (greater than $1x10^5$), there is a range of eddy lengths (Figure 25). Reynold's number is dependent upon the mean flow depth, and the data is from a range of gauge heights at two separate locations

and different protrusions at those locations. Thus, it is not surprising that there is a range of eddy lengths due to the range in flow depths.

Conclusion

Flow resistance is difficult to measure and partition in stream channels. The importance of bank roughness is often overlooked in bank erosion studies, which tend to partition shear stress on the bank via width/depth ratios or other partitioning of the channel (Knight et al, 1984; Flintham and Carling, 1988). Bank hydraulics, however, are influenced by a range of roughness heights, not just the average roughness height or an implied roughness coefficient from visual surveillance. The purpose of this study was to investigate how size and spacing of roughness elements relates to the formation of macroturbulent eddies, which can cause stream bank erosion.

Roughness elements that fall above the roughness cascade are more likely to generate macroturbulent eddies that also plot above the eddy cascade. These eddies can cause erosion along banks on the lee side of the large roughness elements. The results show that Cherry Hill, which experiences the highest degree of bank erosion among the three sites, also has the most roughness elements that fall above the roughness cascade.

The results also show that there is no clear relationship between roughness height and eddy length over a range of flows. However, there does appear to be a critical threshold for Reynold's number which spawns macroturbulent eddies, although more data is needed to define this threshold. The study also used a previous method for predicting eddy length and compared the results with the field measurements. The predicted eddy lengths were two to three times larger than the measured eddies, which is

likely due to interference from other roughness elements and decreasing depth along the bank.

The results illustrate that roughness elements can spawn erosion-causing macroturbulent eddies along natural stream banks without obvious protrusions. This suggests that studies that measure hydraulic erosion by relating stream bank retreat and shear stress partitioning (Julian and Torres, 2005) may be ascribing erosion associated with macroturbulent eddies to particle erosion by applied bank shear stresses.

This study also suggests a method for determining when roughness elements are too large and isolated to generate roughness, and will instead generate eddies. This is of particular importance to stream restoration practices in which tree planting and rootwad placement are common practices. Restoration projects have failed due to that lack of understanding of bank roughness. In one study, the replacement of floodplain trees with widely-spaced rootwads caused eddy scour and failure of the channel system (Smith and Prestegaard, 2005**)**

Summary and Implications

Stream bank erosion rates and the stabilization of channel width are important processes in regards to stream restoration but are poorly understood. In this thesis, two approaches to the understanding of bank erosion processes were pursued; 1) An investigation of the role of channel curvature on downstream bank hydraulics, and 2) An evaluation of the role of bank roughness elements in the formation of macroturbulent eddies and bank erosion. The objectives of the research were to 1) Determine if river segments can be divided into straight reaches and curved reaches and if different bank erosion prediction approaches may be applied to each; 2) Create a method for physically measuring bank roughness that can be used to evaluate bank roughness distributions; and 3) Determine the conditions under which stream bank roughness, specifically the size and spacing of bank protrusions, generates stable, macro-turbulent eddies that affect near bank velocities, shear stress, and bank erosion.

The investigation of the whether rivers can be divided into straight and curved segments was conducted using data from the East Fork River, Wyoming (Prestegaard, 1982). Data from Prestegaard (1982) was used to calculate bank shear stress values using two separate methods. The Einstein method (Einstein and Barbarossa, 1951), which uses measured distributions of velocity in the channel cross section to partition the shear velocity into bank and bed components, was compared with the Carling method (Flintham and Carling, 1988), which uses the channel dimensions to partition the shear stress into bank and bed components. The study reach appears straight in aerial photographs, but there is a meander bend approximately 25 meters upstream of the first

gauged transect. If the downstream hydraulics were not affected by the upstream curvature, then the Carling method should yield similar bank shear stress values as the Einstein method.

The results for this study indicate that although the study reach along the East Fork River appears to be straight, upstream morphology still influences the hydraulics along the banks up to 100 meters downstream, and the Carling method does not predict similar bank shear stress values at the furthest downstream gauged transect. Thus, it is concluded that curved river segments affect the shear stress distributions of nearby, straight reaches. As a result, using a shear stress prediction approach that assumes a reach to be straight on a section of river downstream of a meander bend will not yield accurate shear stress values. However, the same approach may still reveal the extent of a meander bend's influence on downstream bank hydraulics.

The East Fork River was used in this study because it is a simple channel with low bank roughness and uniform bed roughness along the study reach. However, many other streams are subject to hydraulic disturbances beyond channel curvature with the generation of macroturbulent eddies due to large stream bank roughness elements.

In order to examine the role of stream bank roughness in the generation of macroturbulent eddies, a method for physically measuring bank roughness was developed. The study sites included natural and stabilized sections of the Anacostia River, a region where urbanization has exerted significant stresses on the channel, resulting in high rates of bank erosion (Behrns, 2007). During high flows, macroturbulent eddies formed at isolated roughness elements. These eddy lengths were measured and compared with the physical roughness size at the gauge height at the time

of the eddy generation. Sites containing roughness elements that fell above the roughness cascade are more likely to produce eddies that fall above the eddy cascade, which are large, stable, and can cause erosion. These eddy lengths were then compared with eddy lengths predicted from Raupach's (1992) study of drag partition on rough surfaces. The predicted eddy lengths were compared with the measured eddy lengths and analyzed alongside the hydrologic data to evaluate conditions under which macroturbulent eddies occur.

A comparison of bank erosion rates among the three reaches indicates that the site which experiences the highest degree of bank erosion among the three sites also has the most roughness elements that fall above the roughness cascade. This suggests that macroturbulent eddies may play a significant role in bank erosion in these straight reaches. Although there is no simple relationship between roughness height and eddy length over the range of measured flows, there does appear to be a critical Reynold's number which spawns macroturbulent eddies at 1×10^5. This threshold could be defined by the hydraulic characteristics of these sites, and more data are needed to define this threshold.

The results from the macroturbulent eddy study illustrate that roughness elements can spawn erosion-causing, macroturbulent eddies along natural stream banks without obvious protrusions. This is important as it suggests that bank erosion studies which measure hydraulic erosion by relating stream bank retreat and shear stress partitioning (Julian and Torres, 2005) may be ascribing erosion associated with macroturbulent eddies to particle erosion by applied bank shear stress.

The results of this study suggest that bank roughness is best described as a distribution of roughness heights rather than an average roughness value or an estimated Mannning's n value. In this study, I present a method for determining when roughness elements are large and isolated enough to generate stable macroturbulent eddies. The approach to roughness evaluation in this study is of particular importance to stream restoration practices in which tree planting and rootwad placement are important components. A number of restoration projects have failed due to bank erosion, which may be related to the lack of understanding of bank roughness. In one study, the replacement of floodplain trees with widely-spaced rootwads caused eddy scour and bank erosion, which undermined the structural elements emplaced in the restoration effort. (Smith and Prestegaard, 2005). Any stream restoration project that changes the roughness along the banks of the restored reach should consider the size and spacing of the roughness elements in regards to macroturbulent eddy creation. This thesis used Raupach's (1992) method for eddy-length prediction, but found that it overestimated the length by a factor of two to three times the actual measured eddy length. Houghton (1997) used Fourier analysis of velocity data to predict eddy length scales, and also found that the method generated much larger length scales than those observed in the field. Therefore, it appears more research is needed in the realm of eddy length prediction in order to best estimate eddy formation in stream restoration.

This research presents a method for detecting the erosion-causing elements (high bank shear stress and macroturbulent eddies) in a stream system and where they may fit in a hierarchy of erosion-causing mechanisms. Results from this study and previous research indicate a potential hierarchy of erosion mechanisms as follows (from greatest to

least influence): 1) channel curvature, 2) channel central bars, 3) alternate bars, 4) bank roughness that generates macroturbulent eddies, and 5) shear stress partitioning in straight reaches. The relative influence of each control, however, changes with flow depth, which governs Reynold's number and shear stress at a stream location. For low flows, channel curvature, mid-channel bars, and alternate bars are the main erosion-causing factors. Bank roughness is not included in this hierarchy as the largest bank roughness elements generated by vegetation are found at near bankfull conditions. At low flow, alternate bars are the largest roughness component along banks. Under bankfull conditions, channel curvature, mid-channel bars, and macroturblence-generating bank roughness play significant roles in bank erosion. Alternate bars are commonly submerged during bankfull flows and the flow often straightens over the reach. Large bank roughness elements like rootwads and tree trunks are the largest roughness component along banks, and these contribute to local scour.

This hypothetical hierarchy of erosion factors can be used to predict possible "hot spots" for bank erosion. Using an aerial photograph of a reach, one may be able to identify alternate bars, bank curvature, and other erosion contributing features. Bank roughness characteristics may need to be identified from field data. The results from research can be used to highlight possible areas that may experience above average rates of bank erosion, such as the outer bank downstream of a meander bend or the leeside of an isolated tree along a stream bank. It is not possible, however, to predict erosion rates from these methods alone. This presents opportunity for future research in stream restoration and design.

References

Abad, J.D., Rhoads, B.L, Guneralp, I., Garcia, M.H. 2008. Flow structure at different stages in a meander-bend with bendway weirs. Journal of Hydraulic Engineering 134: 1052-1063.

Abernethy, B., Rutherford, I.D. 1998. Where along a river's length will vegetation most effectively stabilize stream banks. Geomorphology 23: 55-75.

ASCE Task Committee on Hydraulics, Bank Mechanisms, and Modeling of River Width Adjustment, 1998. River width adjustment: I. Processes and mechanisms. Journal of Hydraulic Engineering 124: 881-902.

Bagnold, R.A. 1960. Some aspects of river meanders. U.S. Geological Survey Prof. Paper 282-E.

Bauer, B.O., Schmidt, J.C. 1993. Waves and sandbar erosion in the Grand Canyon: applying coastal theory to a fluvial system. Annals of the Association of American Geographers 83: 475-497.

Bathhurst, J. C. 1993. Flow resistance through the channel network. New York: John Wiley and Sons, Ltd: 69-98.

Behrns, K. 2007. Evaluation of channel adjustments to urbanization on the Paint Branch Stream System. Unpublished Senior Thesis Paper, University of Maryland College Park.

Bohn, C. 1989. Management of winter soil temperatures to control streambank erosion. Practical Appraoches to Riparian Resource Management: An Educational Workshop. American Fisheries Society, Bethesda, MD: 69-71.

Bridge, J.S. 2003. Rivers and floodplains: forms, processes, and sedimentary record. Blackwell Science Ltd. Malden, MA.

Carrasco, A., Vionnet, C.A. 2004. Separation of scales on a broad, shallow, turbulent flow. Journal of Hydraulic Research 42: 630-638.

Carter, C.L., Anderson, R.S. 2006. Fluvial erosion of physically modeled abrasion dominated slot canyons. Geomorphology 81: 89-113.

Duan, J.G. 2005. Analytical approach to calculate rate of bank erosion. Journal of Hydraulic Engineering 131: 980-990.

Dun, R.W. 2006. Reducing uncertainty in the hydraulic analysis of canals. Proceedings of

the Institution of Civil Engineers – Water Management 159: 211-224.

Eaton, B.C., Millar, R.G. 2004. Optimal alluvial channel width under a bank stability constraint.. Geomorphology 62: 35+45.

Einstein, H.A., Barbarossa, N.L. 1951. River Channel Roughness. Transactions of the American Society of Civil Engineers 117: 1121-1132.

Flintham, I.P., Carling, P.A. 1988. The prediction of mean bed and wall boundary shear in uniform and compositely rough channels. International Conference on River Regime: 267-287.

Florsheim, J.L., Mount, J.F., Chin, A. 2008. Bank erosion as a desirable attribute of rivers. Bioscience 58: 519-529.

Hammer, T.R. 1972. Stream channel enlargement due to urbanization. Water Resources Research 8: 1530-1540.

Hooke, J.M. 1980. Magnitude and distribution of rates of river bank erosion. Earth Surface Processes 5: 143-157.

Houghton, K.K. 1997. Techniques for measuring and analyzing turbulence in natural channels. Master of Science Thesis, University of Maryland College Park.

Hudson, P.F., Kesel, R.H. 2000. Channel migration and meander-bend curvature in the lower Mississippi River prior to major human modification. Geology 28: 531-534.

Jang, C., Shimizu, Y. 2005. Numerical simulation of relatively wide, shallow channels with erodible banks. Journal of Hydraulic Engineering131: 565-575.

Jarvela, J. 2002. Flow resistance of flexible and stiff vegetation: a flume study with natural plants. Journal of Hyrdology 269: 44-54.

Julian, J.P., Torres, R. 2005. Hydraulic erosion of cohesive riverbanks. Geomorphology: 76: 193-206.

Knight, D.W., Demetrious, J.D., Hamed, M.E. 1984. Boundary shear in smooth rectangular channels. Journal of Hydraulic Enigneering ASCE 110: 405-422.

Kolmogorov, A.N. 1962. A refinement of previous hypotheses concerning the local structure of turbulence in a viscous incompressible fluid at high Reynolds number. Journal of Fluid Mechanics 13: 82-85.

Kouwen, N., Fathi-Moghadam, M. 2000. Friction factors for coniferous trees along rivers. Journal of Hydraulic Engineering – ASCE 126: 732-740.

Lawler, D.M. 1995. The impact of scale on the processes of channel-side sediment supply: a conceptual model. Effects of Scale on Interpretation and management of Sediment and Water Quality (Proc. Of a Boulder Symp.) IAHS Publ., 226. Boulder, CO: 175-184.

Leighly, J. 1936. Meandering arroyos of the dry southwest. Geographical Review 26: 270-282.

Leopold, L.B., Emmett, W.W. 1997. Bedload and river hydraulics – inferences from the East Fork River, Wyoming. U.S. Geological Survey Prof. Paper 1583.

Leopold, L.B., Maddock, T., Jr. 1953. The hydraulic geometry of stream channels and some physiographic implications. U.S. Geological Survey Prof. Paper 252.

Leopold, L.B., Wolman, M.G. 1957. Channel patterns: braided, meandering, and straight. U.S. Geological Survey Prof. Paper 282B.

Leopold, L.B., Wolman, M.G. 1960. River meanders. Geological Society of America Bulletin 71: 769-794.

Meneveau, C., Sreenivasan, K.R. 1987. Simple multifractal cascade model for fully developed turbulence. Physical Review Letters 59: 1424-1427.

Nadan, P., Rameshwaran, P., Mountford, O., Robertson, C. 2006. The influence of macrophyte growth, typical of eutrophic conditions, on ricer flow velocities and turbulence production. Hydrological Processes 20: 3915-3938.

Nanson, G.C., Hickin, E.J. 1983. Channel migration and incision on the Beatton River. American Society of Civil Engineers Proceedings, Journal Hydraulic Engineering 109: 327-337.

Nanson, G.C., Hickin, E.J. 1986. A statistical analysis of bank erosion and channel migration in western Canada. Geological Society of America Bulletin 97: 497-504.

Odgaard, A.J. 1989. Meander flow model I: development. Journal of Hydraulic Engineering 115(11): 1433-1450.

Perumal, M. Moramarco, T., Sahoo, B., Barbetta, S. 2007. A methodology for discharge estimation and rating curve development at ungauged river sites. Water Resouces Research 43: W02412.

Prestegaard, K.L., 1982, Flow resistance in gravel bed and sand bed streams: University of California Ph.D. dissertation.

Ritter, D.F., Kochel, R.C., Miller, J.R. 2002. Process Geomorphology: 4th Edition.

McGraw-Hill. New York, NY.

Raupach, M.R. 1992. Drag and drag partition on rough surfaces. Boundary Layer Meteorology 60: 375-395.

Ritter, D.F., Kochel, R.C., Miller, J.R. 2002. Process Geomorphology: 4th Edition. McGraw-Hill. New York, NY: 190-206.

Smith, S.M., Prestegaard, K.L. 2006. Hydraulic performance of a morphology-based stream channel design. Water Resources Research 41: W11413.

Sutton, S.F., Neuman, C.M. 2008. Sediment entrainment to the lee of roughness elements: effects of vortical structures. Journal of Geophysical Research 113: F02S09.

Thorne, C.R. 1991. Bank erosion and meander migration of the Red and Mississippi Rivers, USA. Hydrology for the Water Management of Large River Basins. Proc. symposium, Vienna: 301-313.

Wu, F.S. 2008. Characteristics of flow resistance in open channels with non-submerged rigid vegetation. Journal of Hydrodynamics 20: 239-245.

Zen, E.A., Prestegaard, K.L. 1994. Possible hydraulic significance of two kinds of potholes – examples from the Paleo-Potomac River. Geology 22: 47-50.